NATIONAL TECHNICAL UNIVERSITY OF ATHENS
SCHOOL OF NAVAL ARCHITECTURE & MARINE ENGINEERING
DIVISION OF MARINE ENGINEERING

DIPLOMA THESIS

The influence of manufacturing tolerances on the performance of fluid film thrust bearings

ZOUPAS LOUKAS

Thesis Committee:

Supervisor: **C.I. Papadopoulos, Assistant Professor NTUA**

Members: **L. Kaiktsis, Associate Professor NTUA**

G. Papalambrou, Assistant Professor NTUA

Athens, June 2017

ΕΘΝΙΚΟ ΜΕΤΣΟΒΙΟ ΠΟΛΥΤΕΧΝΕΙΟ
ΣΧΟΛΗ ΝΑΥΠΗΓΩΝ ΜΗΧΑΝΟΛΟΓΩΝ ΜΗΧΑΝΙΚΩΝ
ΤΟΜΕΑΣ ΝΑΥΤΙΚΗΣ ΜΗΧΑΝΟΛΟΓΙΑΣ

ΔΙΠΛΩΜΑΤΙΚΗ ΕΡΓΑΣΙΑ

Επίδραση κατασκευαστικών λαθών μορφής στην απόδοση αυτορυθμιζόμενων ωστικών εδράνων

ΖΟΥΠΑΣ ΛΟΥΚΑΣ

Εξεταστική επιτροπή:

Επιβλέπων: **Χ.Ι. Παπαδόπουλος, Επίκουρος Καθηγητής ΕΜΠ**

Μέλη: **Λ. Καϊκτσής, Αναπληρωτής Καθηγητής ΕΜΠ**

Γ. Παπαλάμπρου, Επίκουρος Καθηγητής ΕΜΠ

Αθήνα, Ιούνιος 2017

Table of Contents

Acknowledgements

First of all, I would like to thank my supervisor, Assistant Professor Christos Papadopoulos for his persistence and patience that showed throughout every step of the present thesis. He inspired me, advised me and motivated me, and I want to express my deepest gratitude to him for developing a very good collaboration environment.

In addition, I owe a great thank to Mr. Vasilis Zouzoulas, Naval Architect and Marine Engineer NTUA for his guidance in developing a CFD model using ANSYS CFX solver.

Furthermore, I would to thank Professors Michal Wodtke and Michal Wasilczuk for the data they provided and for their kind collaboration.

Last but not least, I want to thank my family for giving me the chance for an education and providing me all the means to accomplish my goals. Also, important contribution have my friends, fellow students and my cousins who were there for me and supported me every single time.

Σύνοψη

Η τριβή είναι ο κύριος λόγος που τα μηχανολογικά συστήματα παρουσιάζουν απώλειες ενέργειας. Τέτοια συστήματα υπάρχουν στα πλοία, τόσο στην κύρια μηχανή (έδρανα, ελατήρια εμβόλων, κ.λπ.), όσο και σε ολόκληρο το αξονικό σύστημα με το οποίο συνδέεται η κύρια μηχανή. Για να ελαττωθούν αυτές οι απώλειες, καθώς και η συνεπαγόμενη φθορά των εμπλεκόμενων εξαρτημάτων, συνήθως χρησιμοποιούνται λιπαντικά μέσα μεταξύ των αλληλεπιδρουσών επιφανειών (π.χ στα ακτινικά έδρανα του πλοίου, στο ωστικό έδρανο του πλοίου, κ.α).

Η παρούσα εργασία, μελετά τις απώλειες τριβής σε ωστικά έδρανα. Ωστικά έδρανα χρησιμοποιούνται κατά κόρον στα πλοία όπου κύριος στόχος τους είναι η μετάδοση των μεγάλων αξονικών δυνάμεων που δημιουργούνται από την έλικα του πλοίου προς τη γάστρα αυτού. Τα ωστικά έδρανα αποτελούνται από δύο βασικά μέρη, το είναι σταθερό (στάτορας) ενώ το άλλο περιστρέφεται (ρότορας). Αξιοποιώντας τις υδροδυναμικές πιέσεις που αναπτύσσονται στο φιλμ του λαδιού μεταξύ του ρότορα και του στάτορα καταφέρνουμε και απομακρύνουμε τα δυο μέρη, ώστε να μην υπάρχει επαφή μετάλλου με μέταλλο κατά τη λειτουργία. Η χρήση των ωστικών εδράνων δεν περιορίζεται μόνο στα ναυτικά συστήματα πρόωσης, αλλά είναι διαδεδομένη και σε περιστρεφόμενες μηχανές όπως αντλίες, συμπιεστές, κ.α.

Στόχος την παρούσας εργασίας είναι η μελέτη και η μοντελοποίηση των κατασκευαστικών σφαλμάτων της επιφάνειας του στάτορα αυτορρυθμιζόμενων ωστικών εδράνων, καθώς και η ποσοτικοποίηση της επίδρασής τους στις παραμέτρους λειτουργίας των εδράνων. Για το λόγο αυτό δημιουργήθηκε ένα τρισδιάστατο γεωμετρικό μοντέλο ενός πέλματος αυτορρυθμιζόμενου ωστικού εδράνου, συμπεριλαμβάνοντας τα σχετικά τμήματα του λιπαντικού ελαίου και του ρότορα. Στο συγκεκριμένο μοντέλο θεωρήθηκε ότι το πέλμα είναι παραμορφωμένο λόγω ελαστικών και θερμικών φορτίσεων. Η παραμόρφωση προσομοιάστηκε ως μία παραβολή (και προς τις δυο διευθύνσεις: ακτινική και περιφερειακή) με κέντρο το σημείο στήριξης του εδράνου. Η μοντελοποίηση των κατασκευαστικών σφαλμάτων στην επιφάνεια του πέλματος έγινε με χρήση ημιτονοειδών συναρτήσεων με διαφορετικό αριθμό ημικυμάτων. Το δημιουργηθέν μοντέλο επιλύθηκε με χρήση κώδικα Υπολογιστικής Ρευστομηχανικής (CFD) για τον υπολογισμό των τριβολογικών παραμέτρων λειτουργίας. Στη συνέχεια, με χρήση ενός προγραμματιστικού εργαλείου, μας δόθηκε η δυνατότητα εύρεσης της θέσης ισορροπίας του πέλματος για δεδομένο ωστικό φορτίο (εξισορρόπηση ώσης και μηδενισμός των ροπών ως προς το σημείο στήριξης). Τέλος, για την εξαγωγή συμπερασμάτων έγινε καταγραφή και ανάλυση σημαντικών παραμέτρων λειτουργίας όπως το ελάχιστο πάχος του λιπαντικού φιλμ, η ροπή τριβής και οι μέγιστες τιμές της πίεσης και της θερμοκρασίας του λιπαντικού. Οι περιπτώσεις κατασκευαστικών σφαλμάτων που εξετάστηκαν αφορούν σε επιφάνειες πέλματος με κοίλη, κυρτή ή κυματοειδή μορφή. Εξετάστηκε η επίδραση των κατασκευαστικών σφαλμάτων για δύο διαφορετικά ωστικά φορτία καθώς και για διαφορετικά πλάτη των κατασκευαστικών σφαλμάτων μεταξύ 0 και 20 μm.

Abstract

Friction is the main reason of energy losses in mechanical systems. Tribological components exist on ships, both in the main engine (crankshaft bearings, piston rings) and in the shaft arrangement with which the engine is coupled (journal bearing, thrust bearing of the ship). In order to minimize these losses, lubricants are used between interactive moving surfaces.

The present thesis is concerned with the study of friction losses in large thrust bearings. Thrust bearings are being used extensively in ships and their main goal is to transfer the large thrust load generated by the propeller to the hull of the vessel. Thrust bearings consist of two major parts, one steady (pad) and one rotatable (collar). Utilizing the hydrodynamic pressure developed by the lubricant film between the stator and rotor, the two parts can be separated, avoiding metal to metal contact. The use of thrust bearing is not limited to marine propulsion systems, but it is used in a plethora of rotating machines such as pumps, compressors, etc.

The aim of the present study is to model the manufacturing errors and examine their influence on the functionality of tilting pad thrust bearings. To this end, a 3D geometric model is generated for a single pad of the bearing, considering also the oil and the respective part of the collar. In this model, it is assumed that the pad is deformed; deformation is simulated as a 3D parabola across two directions namely radially and circumferentially with its center being the pivot point of the pad. Manufacturing errors are simulated as sine waves with different number of waves, varying from 0.5 to 5. Next, a Computational Fluid Dynamic (CFD) model is set up for calculating the tribological characteristics of the system. Using an iterative procedure, the equilibrium position of the bearing is calculated. Finally, attention is given to the trends of essential operating parameters of the bearing, such as minimum oil film thickness, friction torque and maximum values of pressure and temperature of the lubricant.

The studied manufacturing errors examined are (a) concavity, (b) convexity and (c) waviness with one, three or five sinewaves on the pad surface. The cases of concavity and convexity are simulated with the use of a negative or positive half sinewave. Two different thrust loads are considered, whereas manufacturing error amplitudes are varied from 0 to 20 μm.

Nomenclature

A	pad area (m^2)
B	pad width (mm)
c_{pb}	specific heat capacity of babbitt (J/kg.K)
c_{pf}	specific heat capacity of fluid (J/kg.K)
c_{ps}	specific heat capacity of the rotor and pad solids (J/kg.K)
D_i	pad inner diameter (mm)
D_o	pad outer diameter (mm)
Θ_p	pad angle (deg)
Θ_{pivot}	circumferential position of pivot point (deg)
R_{pivot}	pivot radius (mm)
$t_{babbitt}$	babbitt thickness
t_{collar}	collar thickness
t_{pad}	pad thickness
F_f	friction force (N)
T_f	friction torque (Nm)
f	friction coefficient
H	local film thickness (µm)
H_{min}	minimum film thickness (µm)
H_{pivot}	film thickness at pivot location (µm)
L	pad length at bearing mid-sector (mm)
$M_{x,p}$	x- component of torque about pivot point (Nm)
$M_{y,p}$	y- component of torque about pivot point (Nm)
N_p	number of pads
N	rotational speed (RPM)
P	specific load (MPa)
p	pressure (Pa)
Pr	Prandtl number
P_f	power loss due to friction
Q_{feed}	feeding oil flow rate (m^3/s)
Re	local Reynolds number

T	fluid temperature (^oC)
T_{amb}	ambient temperature (^oC)
U	rotor speed at pad mid-sector (m/s): U=ωr
V	fluid velocity vector
W	bearing load capacity / thrust load (N)
λb	thermal conductivity of babbitt (W/m.K)
λf	thermal conductivity of fluid (W/m.K)
λs	thermal conductivity of the rotor and pad solid (W/m.K)
μ	fluid dynamic viscosity (Pa.s)
v	fluid kinematic viscosity (cSt)
ρ	fluid density (kg/m^3)
τ	shear stress (Pa)
ω	rotor angular velocity (rad/s)

List of Figures

List of tables

1. Introduction

1.1 The significance of tribology

Tribology is the branch of science that focuses on friction, wear and lubrication of interacting surfaces that are in relative motion. Friction leads to mechanical power losses and wear; wear is responsible for the degradation of the interacting surfaces leading to pour operation or system malfunction. It is estimated that approximately one third of the worldwide energy consumption is lost into various forms of friction. As a result, the attempt to limit friction losses can lead to significant savings of energy.

An effective way to reduce friction and control wear is by proper lubrication of the interactive surfaces. In particular, the two main issues encountered during the interaction of two solid parts, namely friction and wear, can be tackled if a thin liquid film is interposed between the solid parts that were firstly in contact. The lubricant can be solid, liquid or gas. Generally, the thickness of the lubricant film ranges between 1 and 100 μm. Tribology science is concerned with the design of the interactive surfaces, the optimization of surface treatment and the selection of appropriate lubricant, which can lead to an effective operation of a given arrangement.

The field of marine engineering is no exception and comprises many applications where friction plays a decisive role in overall performance. In ships, important power losses are present in Diesel engines (in piston rings, crankshaft bearings and connecting rod bearings, which in total lead to power losses approximately 5-7.5% of engine BHP), at the shafting system (where losses of 1-2% of BHP in thrust bearing and journal bearings are found), as well as in the gear unit (with losses around 1-2% of BHP), if present. Energy cost due to friction and wear for a particular mechanical component may seem low compared to the total power of the device, but if they are examined under the scope of annual costs of a certain fleet of sea-going vessels, the power savings can reach a considerable value.

1.2 Literature review

In normal operating conditions, a properly designed fluid film bearings operate in the regime of full film lubrication with rubbing surfaces completely separated by a lubricating film. In bearings, the film thickness of the lubricant ranges between micrometers and several dozen micrometers. A common assumption made in theoretical analyses of such bearings is that the sliding surfaces of stator and rotor are geometrically ideal. In practice such an assumption is not realistic due to cutting machine inaccuracies, which always occur despite of precise contemporary manufacturing techniques. Usual tolerances approach the value of 20 micrometers, which is comparable to minimum film thickness.

Apart from machining inaccuracies the shape of sliding surface is also affected, during operation, by bearing loads, which leads to deformations due to temperature distribution and film pressure. In most cases these effects are nowadays taken into

account in theoretical analyses, while the effect of manufacturing imperfections – including roughness, waviness, non-planarity and also wear of the sliding surfaces has been very rarely investigated before. In these few studies the performance of journal bearings with surface imperfections has usually been investigated. For example, Burton [18] and Li with Chen [19] theoretically investigated the influence of surface roughness on bearing properties. Imperfections of bearing geometry, such as ovality, conical shape and errors in circularity were theoretically studied by Pande and Somasundaram [20] and showed changes in gas bearings' characteristics. Wilson [21] proved that theory experimentally. Shelly and Ettles [22] in their study analyzed the influence of transverse and longitudinal surface waviness, with the amplitude of 2.5 μm and circumferential length of 100 μm on journal bearing performance. In [23] and [24] the influence of geometrical imperfections and roughness on load carrying capacity of a radial bearing was tested. Fillon and Bouyer [25] and Litwin [26] were studying the influence of wear of the bush on bearing characteristics, while Dobrica and Fillon [27] theoretically examined the effect of circumferential scratches on bearing operation.

From the above it can be concluded that surfaces of a bearing with manufacturing errors have noticeable influence on bearing performance. Manufacturing errors can affect load carrying capacity, bearing losses and distribution of film pressure and temperature. This is highly important in case of high loaded bearings in which minimum film thickness is small and becomes comparable to the size of the analyzed imperfections

In case of thrust bearings, various modifications of the sliding surface shape were studied. For example, Papadopoulos et al. [28] using CFD examined the effect of microdimples machined on the bearing surface. Fouflias et al. [29] studied the influence of inlet chamfer and a pocket on the performance of a thrust bearing. In [30] and [31] a study was carried out about the influence of the hydrostatic pocket machined in a tilting pad thrust bearing. Despite all these examples, thorough and systematic analysis of the influence of manufacturing imperfections on performance of tilting pad thrust bearings has not been published before. The significant influence of manufacturing errors which can change bearing operation was experimentally shown by Roylance [32], who compared thrust washers with an introduced convexity of 1.9 μm to the flat ones. It was shown that the differences in minimum film thickness were up to 5 - 10 μm, which leads to the conclusion that influence of the sliding surface profile on bearing performance is really important.

1.3 Goal of the present study – Thesis outline

In the present thesis, thrust bearings are modeled using Ansys CFX. A thermohydrodynamic approach is followed, taking into consideration pressure generation and heat dissipation due to shear stresses in the lubricant domain, as well as conjugate heat transfer through the solid domain of the system (rotor and pad solids). Further, elastic/thermal deformations are taken into consideration by appropriately applying a parabolic type of deformation, centered at the pivot location of the bearing pad. Due to limitations imposed by the use of the Reynolds equation, the use of Navier - Stokes equation solvers is imperative for detailed thermohydrodynamic analysis of fluid bearings. In order to calculate the equilibrium position of the thrust bearing (minimum film thickness, rotations about the pivot point), the CFD solver is coupled with an external iterative solver, which is based on the Newton - Raphson method.

The particular aim of the present study is to determine the influence of manufacturing tolerances on the performance of a fluid film thrust bearing. First, the CFD model of the bearing pad is developed and validated against the results of Dąbrowski and Wasilczuk [2]. Then, the model is appropriately extended to simulate different manufacturing errors of the stator surface. In particular, five different cases are being considered:

- Concavity (positive half sinewave)
- Convexity (negative half sinewave)
- Waviness (one, three and five sine wave)

Two different thrust loads (680 and 1360 kN) are studied, whereas error amplitudes are ranged from 5 to 20 microns. Finally, the summarized findings of the study are presented and conclusions are drawn.

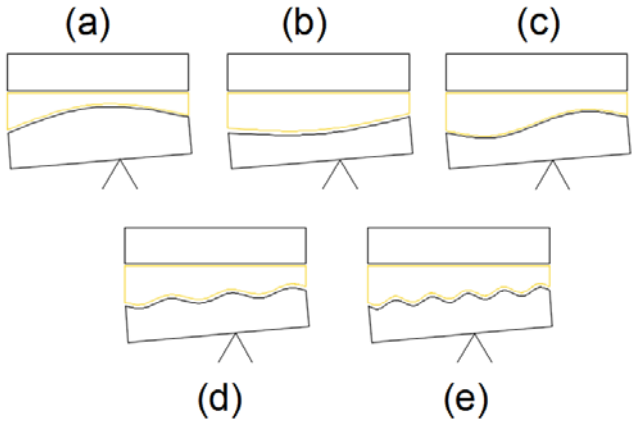

Figure 1 Sketch showing pad with manufacturing errors of: (a) convexity, (b) concavity, (c) one sine wave, (d) three sine waves and (e) five sine waves

2. Thrust Bearing

2.1 Overview

There are two main types of thrust bearings: bearings with rolling elements and fluid film (sliding) bearings. In Marine Engineering, due to enormous sizes and special operating conditions, sliding bearings are mainly used; their function is studied with the use of the hydrodynamic lubrication theory. Generally, bearings are machine elements which support rotating mechanical components. The main objectives of the bearings are the support of radial – axial loads, the minimization of the friction torque between moving parts, the reduction of vibration and noise and the endurance to shock loads. Lubrication of bearings is of great significance, in order to keep friction losses and developing temperatures low.

Bearing with rolling elements can carry a load by placing rolling elements (balls, rollers) between two bearing rings called races. There are five types of rolling elements: balls, cylindrical rollers, tapered rollers, barrel rollers and needle rollers. Typical bearings with rolling elements range in size from 10 mm diameter to a few meters diameter and have load carrying capacity from a few grams to thousands of tonnes.

Thrust bearings can support high static or dynamic loads [4]. As a result they undergo high mechanical wear. Therefore, it is of high importance, to be able to estimate their expected lifetime and determine appropriate preventive maintenance measures. The useful lifetime of a thrust bearing can be quantified in terms of the number of revolutions or the corresponding operating hours (for a given speed), up to which the bearing will work appropriate without any signs of critical wear. In particular the nominal life of a thrust bearing is defined as the absolute number of revolutions, in millions, for which 90% of a series of the same bearings, do not show signs of fatigue. By definition dynamic strength number of a bearing is defined as the constant load (radial for radial bearings and axial for thrust bearings) for which the nominal life of the bearing is 1×10^6 rotations.

Figure 2 (a) Bearing with rolling elements (b) Thrust bearing

Thrust bearings can be either hydrostatic or hydrodynamic, depending on the type of the pressure build up mechanism. Generally, fluid film thrust bearings have lower cost for industrial production compared with rolling bearings of the same load rating.

Furthermore, the design of fluid film thrust bearings is simpler, whereas maintenance requirements are much less and life expectance is by far superior, particularly for the hydrostatic lubricating bearings, due to the existence of a pump which helps bearings to prevent the usual wear during the start/stop function. Also thrust bearings are characterized by increased stiffness when operating at high loads. Finally the bearings are, admittedly, less noisy and provide more smooth operation and, therefore, predominantly used in applications with time varying load and operational requirements with reduced noise and vibration.

On the other hand, fluid film thrust bearings are also characterized by certain disadvantages. One of them is the worsening of operating characteristics (power consumption, stiffness) because of the increasing temperature of the lubricant. Furthermore, due to the usage of lubricant, fluid film thrust bearings can be characterized unsuitable for use in environments in which leakage of lubricant can be disastrous. Finally, as mentioned earlier, fluid film thrust bearings show large amounts of friction losses and high rates of wear during start and stop, consequently they are not suitable for applications where starts and stops are frequent.

2.2 **Hydrodynamic Lubrication**

Osborne Reynolds (1886) was the first who observed that a lubricant flows through a converging wedge between a shaft and a journal bearing. As shown in Figure 3 while oil flows from inlet point to the outlet the oil volume reduces which leads to a pressure build-up. The horizontal plate is usually called rotor and it moves with a constant velocity u_r and the tilt plane is stationary and is called stator.

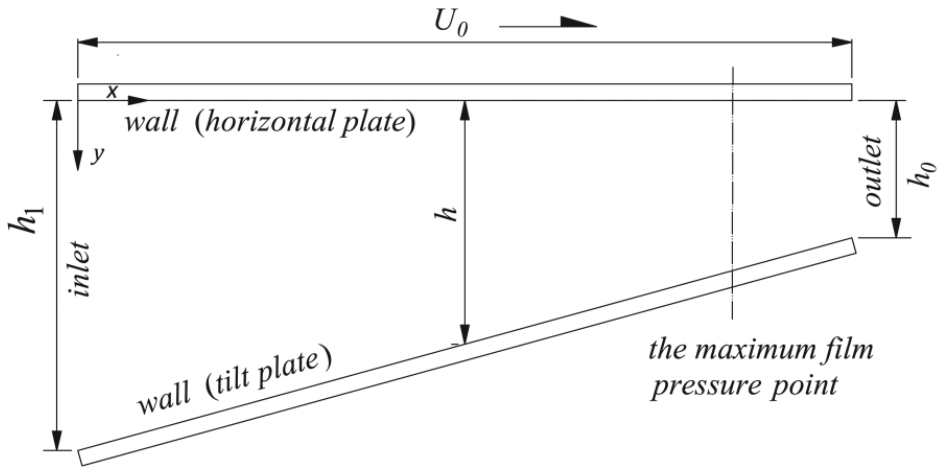

Figure 3 Converging wedge between a pad and a collar

At the surfaces of stator and rotor is being occurred the well-known non slip condition. This means that, the liquid right next to the solid surfaces, it moves with the same tangential velocity of the surface. This is called Couette flow and is a result of the Newtonian rule of liquids. The Newtonian rule states that the shear stress needed to

deform a fluid is linearly proportional to shear strain. Viscosity is the ratio of stress to strain.

$$\tau = \mu \times \frac{\partial u}{\partial z} \quad (1)$$

The theorem of continuity defines that the volume of fluid entering the channel per unit time is equal to the flowing out. Nevertheless, the flow crossing from inlet, outlet depends on the velocity at the boundary, and if velocity is equal then without any pressure build-up, the flow continuity is satisfied. However a thrust bearing with parallel surfaces won't be able to support any load due to the significant ability of a lubricant film to support a load only when pressure build-up in the channel.

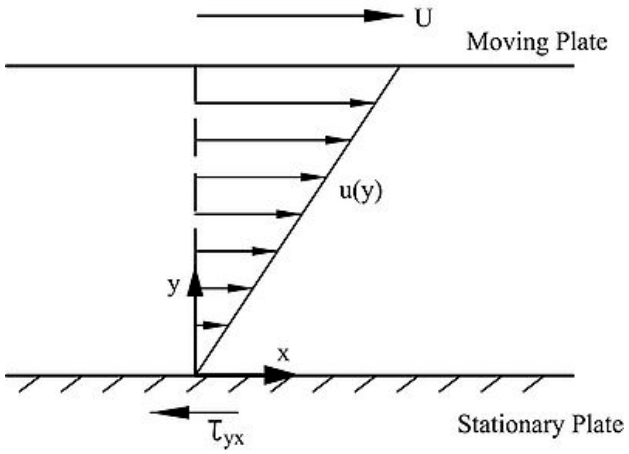

Figure 4 Couette flow in parallel surfaces

Figure 4 shows the flow of two nonparallel plates. The plate width is considered large so as not to take into account the flow in that direction. In first picture (Figure 4(a)), the volume of lubricant at inlet point is greater than the volume at the outlet point. As assumed before, in order to satisfy the flow continuity condition, there is an increase of pressure across the lubricant wedge. Due to the existence of pressure, fluid will try to move from high pressure regions to the lower pressure areas creating a flow pattern called Poiseuille flow (Figure 4(b)). By combining the Couette flow with the Poiseuille flow we get Figure 4(c) which depicts the actual flow pressure and velocities of a typical fixed-inclined thrust bearing.

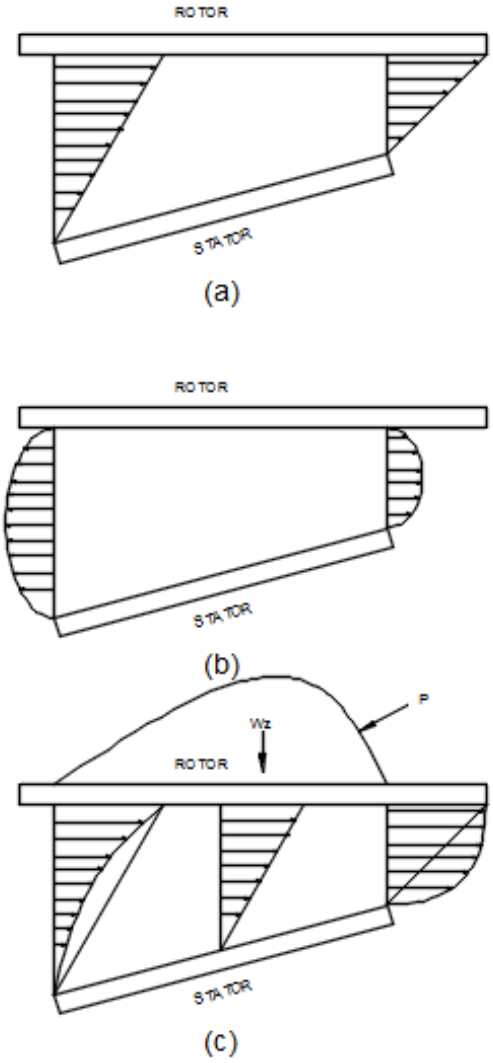

Figure 5 Typical flow and pressure field of thrust bearings

2.3 Mathematical approach

2.3.1 Governing equations

Navier Stokes are the governing equations of heat dissipation and viscous flow in fluid mechanics. Navier Stokes equations are an extension of Euler equations which refer to inviscid flow. They refers to:

- Conservation of momentum equations
- Continuity equation for conservation of mass
- Conservation of energy

The externally applied forces cause fluid flow. These forces are pressure differences, shear, gravity, surface tension and rotation (driving forces). Driving forces can be separated in two different categories: those that are proportional to area (surface forces) and those that are proportional to volume (body forces). The forces that are related to body are gravitational, magnetic-electric fields and centrifugal, while the fluid static pressure and viscous stresses are related to surface forces. About shear force, it is created by the motion of a rigid wall relative to the fluid.

Momentum equations

For an arbitrary portion of the fluid if we apply the Newton's second law (conservation of Momentum), we get, from Navier Stokes equations, the general vector-form:

$$\frac{\partial \rho V}{\partial t} + \nabla \times (\rho V \otimes V) = -\nabla p + \nabla \tau + S \qquad (2)$$

where,

V: velocity vector

ρ: fluid density

p: pressure

τ: total stress tensor

S: represents body forces acting on the fluid (per unit volume)

The **S** vector field most of the times consists of gravity, but in many cases it may be neglected. This assumption, generally, is valid only for hydrodynamic lubrication problems, consequently fluid motion is the result of a pressure field and a shear arising by the imposed motion.

For Newtonian incompressible fluid flows (for Mach numbers lower than the value of 0.3), the Eq.(2) is simplified as:

$$\rho \left(\frac{\partial V}{\partial t} + V \cdot \nabla V \right) = -\nabla p + \nabla \tau \qquad (3)$$

Eq.(3) can separate into three equations for each direction (x, y, z) with the velocity vector as $V = (u, v, w)$

X direction

$$\rho\left(\frac{\partial u}{\partial t}+u\frac{\partial u}{\partial x}+v\frac{\partial u}{\partial y}+w\frac{\partial u}{\partial z}\right)=-\frac{\partial p}{\partial x}+2\frac{\partial}{\partial x}\left(\mu\frac{\partial u}{\partial x}\right)+\frac{\partial}{\partial y}\left[\mu\left(\frac{\partial u}{\partial y}+\frac{\partial v}{\partial x}\right)\right]+\frac{\partial}{\partial z}\left[\mu\left(\frac{\partial u}{\partial z}+\frac{\partial w}{\partial x}\right)\right]-\frac{2}{3}\frac{\partial}{\partial x}(\mu\nabla V) \quad (4)$$

Y direction

$$\rho\left(\frac{\partial v}{\partial t}+u\frac{\partial v}{\partial x}+v\frac{\partial v}{\partial y}+w\frac{\partial v}{\partial z}\right)=-\frac{\partial p}{\partial y}+\frac{\partial}{\partial x}\left[\mu\left(\frac{\partial u}{\partial y}+\frac{\partial v}{\partial x}\right)\right]+2\frac{\partial}{\partial y}\left[\mu\frac{\partial v}{\partial y}\right]+\frac{\partial}{\partial z}\left[\mu\left(\frac{\partial v}{\partial z}+\frac{\partial w}{\partial y}\right)\right]-\frac{2}{3}\frac{\partial}{\partial y}(\mu\nabla V) \quad (5)$$

Z direction

$$\rho\left(\frac{\partial w}{\partial t}+u\frac{\partial w}{\partial x}+v\frac{\partial w}{\partial y}+w\frac{\partial w}{\partial z}\right)=-\frac{\partial p}{\partial z}+\frac{\partial}{\partial x}\left[\mu\left(\frac{\partial u}{\partial z}+\frac{\partial v}{\partial x}\right)\right]+\frac{\partial}{\partial y}\left[\mu\left(\frac{\partial v}{\partial z}+\frac{\partial w}{\partial y}\right)\right]+2\frac{\partial}{\partial z}\left(\mu\frac{\partial w}{\partial z}\right)-\frac{2}{3}\frac{\partial}{\partial z}(\mu\nabla V) \quad (6)$$

Continuity equation

Conservation of mass is necessary, regardless of the flow assumptions. This is achieved with the continuity equations (in general form):

$$\frac{\partial\rho}{\partial t}+\nabla(\rho V)\equiv\frac{\partial\rho}{\partial t}+\frac{\partial(\rho u)}{\partial x}+\frac{\partial(\rho v)}{\partial y}+\frac{\partial(\rho w)}{\partial z}=0 \quad (7)$$

But **for the case of** incompressible flow, density is constant, so the mass continuity equations is simplified to a volume continuity equation:

$$\frac{\partial u}{\partial x}+\frac{\partial v}{\partial y}+\frac{\partial w}{\partial z}=0 \quad (8)$$

Energy equation

At a differential control volume in a moving fluid in steady conditions, the conservation of energy applied, denotes that net rate at which energy goes into a control volume, plus the rate at which heat is being added, minus the rate at which work is done by the fluid, is equal to zero. After manipulation, the thermal energy equation gets the form:

$$\rho c_{pf}\left(u\frac{\partial T}{\partial x}+v\frac{\partial T}{\partial y}+w\frac{\partial T}{\partial z}\right)=\lambda_f\left(\frac{\partial^2 T}{\partial x^2}+\frac{\partial^2 T}{\partial y^2}+\frac{\partial^2 T}{\partial z^2}\right)-\mu\Phi+q \quad (9)$$

where,

λ_f: thermal conductivity of the fluid

c_{pf}: specific heat capacity of the fluid

q=0: heat generation

Φ: viscous dissipation

$$\Phi=2\left[\left(\frac{\partial u}{\partial x}\right)^2+\left(\frac{\partial u}{\partial y}\right)^2+\left(\frac{\partial u}{\partial z}\right)^2\right]+\left(\frac{\partial u}{\partial y}+\frac{\partial v}{\partial x}\right)^2+\left(\frac{\partial v}{\partial z}+\frac{\partial w}{\partial y}\right)^2+\left(\frac{\partial w}{\partial x}+\frac{\partial u}{\partial z}\right)^2 \quad (10)$$

The terms at the left-hand side of the equation account for the net rate at which thermal energy go away the control volume duet to bulk fluid motion. On the other hand, at the right side of the equation, the terms account for net inflow of energy due to heat generation, conduction, viscous dissipation. The net rate that mechanical work is irreversible converted to thermal energy due to viscous effects in fluid is represented by viscous dissipation. The term of "q" (heat generation) express conversion from other forms of energy (electrical, chemical, nuclear, electromagnetic) to total energy.

Heat transfer equations

Heat is transmitted by means of convection and conduction. Convection exists due to intensive flow, conduction takes place in all structural components of the bearing.

Heat that is transferred due to the phenomenon of conduction obeys Fourier's law (expressed for a three dimension field):

$$q'' = -\lambda_s \mathrm{x} \nabla \mathrm{x} \mathrm{T} = -\lambda_s \left(\frac{\partial T}{\partial x} + \frac{\partial T}{\partial y} + \frac{\partial T}{\partial z}\right) \tag{11}$$

where,

q'': heat flux

λ_s: solid thermal conductivity

Respectively, convectional heat transfer can be calculated by:

$$q'' = a(T_{wall} - T_{bulk}) \tag{12}$$

The "α" factor represents the convection coefficient (W/m^{2}K) and depends on the relation between thicknesses of temperature and velocity boundary layers (Prandtl number **Pr**) and also the type of flow (turbulent or laminar) which is expressed by the Reynolds number.

$$Pr = \frac{\nu}{\alpha} = \frac{c_p \mu}{\lambda} \sim \frac{\text{viscous diffusion rate}}{\text{thermal diffusion rate}} \tag{13}$$

$$Re = \frac{\rho U h}{v} \sim \frac{\text{inertial forces}}{\text{viscous forces}} \tag{14}$$

State equation

The viscosity of the liquid is a function of the temperature and is represented by empirical models or simplified mathematics which are valid only for a small temperature range and for selected fluids. The simplest model was first proposed by Reynolds (1886):

$$\mu(T) = \mu_0 e^{(-bT)} \tag{15}$$

Where b, μ_0 are coefficients

A more accurate relationship between viscosity and temperature for hydrocarbons and petroleum based oils is given by McCoull-Walther's equation:

$$loglog(v + 0.6) = A - Blog(T) \tag{16}$$

where,

v: kinematic viscosity

A, B: constants for a given liquid

From Eq.(16) higher temperatures result in lower viscosities.

The dynamic viscosity (or absolute) is obtained by multiplying fluid's mass density with its kinetic viscosity.

$$\mu = \rho \cdot \nu = \rho \cdot \left(10^{10^{A-Blog(T)}} - 0{,}6\right) \quad (17)$$

Eventually, the effect of temperature and pressure in liquid's density is small, for this reason the density is considered to be constant in the present thesis.

$$\rho(p,T) \cong constant \quad (18)$$

Summary of governing equations

Eqs. (4)-(6),(8-9),(17) comprise a six by six system with the unknowns (u,v,w,p,μ,T) which completely describes the problem of hydrodynamic lubrication. With the help of Navier Stokes equations the velocity field is solved but other quantities of physical significance may be derived. The values of pressure, flow rate or drag force are usually of high interest.

2.3.2 Reynolds approximation

In every fluid flow problem the Navier Stokes equations are nonlinear partial differential equations, which makes them really difficult to solve. Even in the simplest case of laminar flow of an incompressible fluid also nonlinearity exists due to the change in velocity over position (convective acceleration).

On the other hand, in case of one-dimensional flow we can simplify the equations to linear form which leads to a straight forward solution. The person who reached a closed form solution of hydrodynamic lubrication problem by using linear form of Navier Stokes equation coupled with the continuity assumption was Osborne Reynolds. However, he had to take some assumptions, the most important of which are:

a. Laminar and incompressible flow assumption.
b. Zero pressure gradient through the oil film thickness
c. Infinite width approximation
d. Isothermal flow

There are two types of bearing, the fixed and tilting pads. The Reynolds equation, most of the times, is written in cylindrical coordinates. Nevertheless, due to the film thickness is small in comparison with the radius of curvature in thrust bearings, the Reynolds equation is written in Cartesian coordinates without having significant loss

of accuracy. Figure 5 shows a typical 3D sketch of thrust bearing and how the corresponding reference coordinate system has been taken for calculations.

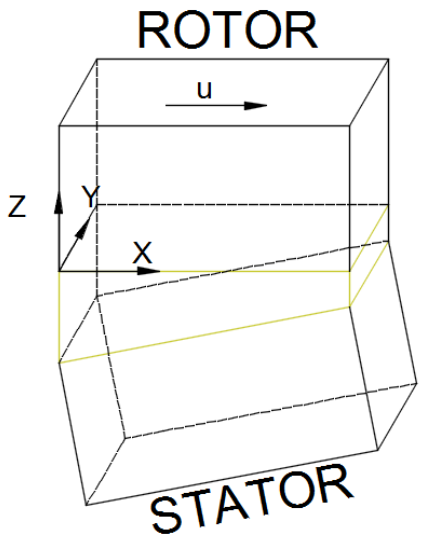

Figure 6 3D sketch of a thrust bearing and how coordinate system has been taken for calculations

The Navier Stokes equations are written, taking into account the above assumptions:

X direction

$$\rho\left(u\frac{\partial u}{\partial x}+w\frac{\partial u}{\partial z}\right)=-\frac{\partial p}{\partial x}+\mu\left(\frac{\partial^2 u}{\partial x^2}+\frac{\partial^2 u}{\partial z^2}\right) \tag{19}$$

Z direction

$$\rho\left(u\frac{\partial w}{\partial x}+w\frac{\partial w}{\partial z}\right)=-\frac{\partial p}{\partial z}+\mu\left(\frac{\partial^2 w}{\partial x^2}+\frac{\partial^2 w}{\partial z^2}\right) \tag{20}$$

We want to get the above equations into dimensionless form so we use:

- L_x : length in x direction [m]
- L_z : length in z direction [m]
- u_0 : velocity in x direction [m/s]
- w_0 : velocity in z direction [m/s]
- ρ_0 : density [kg/m^3]
- n_0 : dynamic viscosity [Ns/m^2]
- p_0 : pressure [Pa]

Using the above parameters the non-dimensional parameters are:

$$x^*=\frac{x}{L_x}\ ,\ z^*=\frac{z}{L_z}\ ,\ u^*=\frac{u}{u_0}\ ,\ w^*=\frac{L_x}{L_z}\cdot\frac{w}{u_0},\rho^*=\frac{\rho}{\rho_0}\ ,\ \mu^*=\frac{\mu}{\mu_0}\ ,\ p^*=\frac{p}{p_0} \tag{21}$$

The velocity w^* is scaled in order to get the same Reynolds number in the two directions (X, Z). Using the dimensionless into Eq. (19):

$$\frac{1}{L_x}u_0^2u^*\frac{\partial u^*}{\partial x^*}+\frac{1}{L_x}u_0^2w^*\frac{\partial u^*}{\partial z^*}=-\frac{1}{L_x}\frac{p_0}{\rho_0}\frac{\partial p^*}{\partial x^*}\frac{1}{\rho^*}+\frac{\mu_0}{\rho_0}\left(\frac{u_0}{L_x^2}\frac{\partial^2 u^*}{\partial x^{*2}}+\frac{u_0}{L_z^2}\frac{\partial^2 u^*}{\partial z^{*2}}\right)\frac{\mu^*}{\rho^*} \tag{22}$$

Rearranging and multiplying by L_x/u_0^2

$$u^* \frac{\partial u^*}{\partial x^*} + w^* \frac{\partial u^*}{\partial z^*} = -\frac{p_0}{\rho_0} \frac{1}{u_0^2} \frac{\partial p^*}{\partial x^*} \frac{1}{\rho^*} + \frac{\mu_0 L_x}{\rho_0 u_0 L_z^2} \left[\left(\frac{L_z}{L_x} \right)^2 \frac{\partial^2 u^*}{\partial x^{*2}} + \frac{\partial^2 u^*}{\partial z^{*2}} \right] \frac{\mu^*}{\rho^*} \tag{23}$$

where the inverted Reynolds number appears:

$$1/Re = \frac{\mu_0 L_x}{\rho_0 u_0 L_z^2} \tag{24}$$

By defining the reference pressure as:

$$p_0 = \frac{\mu_0 u_0 L_x}{L_z^2} \tag{25}$$

we get, the non-dimensional form in x direction

$$u^* \frac{\partial u^*}{\partial x^*} + w^* \frac{\partial u^*}{\partial z^*} = -\frac{1}{Re^*} \frac{\partial p^*}{\partial x^*} \frac{1}{\rho^*} + \frac{1}{Re^*} \left[\left(\frac{L_z}{L_x} \right)^2 \frac{\partial^2 u^*}{\partial x^{*2}} + \frac{\partial^2 u^*}{\partial z^{*2}} \right] \frac{\mu^*}{\rho^*} \tag{26}$$

In a similar way, the Eq. (20) yields:

$$u^* \frac{\partial w^*}{\partial x^*} + w^* \frac{\partial w^*}{\partial z^*} = -\frac{1}{Re^*} \left(\frac{L_z}{L_x} \right)^2 \frac{\partial p^*}{\partial x^*} \frac{1}{\rho^*} + \frac{1}{Re^*} \left[\left(\frac{L_z}{L_x} \right)^2 \frac{\partial^2 w^*}{\partial x^{*2}} + \frac{\partial^2 w^*}{\partial z^{*2}} \right] \frac{\mu^*}{\rho^*} \tag{27}$$

From assumption “c” $L_z << L_x$ so we can neglect L_z/L_x (in Eq. (26)) :

$$Re^* u^* \frac{\partial u^*}{\partial x^*} + Re^* w^* \frac{\partial u^*}{\partial z^*} = -\frac{\partial p^*}{\partial x^*} \frac{1}{\rho^*} + \frac{\partial^2 u^*}{\partial z^{*2}} \frac{\mu^*}{\rho^*} \tag{28}$$

Creeping flow is what fluid flow is in lubricating contacts, therefore inertial phenomena which are expressed through the terms multiplied with the Reynolds number in Eq. (28) can be neglected:

$$\frac{\partial p^*}{\partial x^*} = \mu^* \frac{\partial^2 u^*}{\partial z^{*2}} \tag{29}$$

Integrating twice, the last equation, with respect to z we get:

$$u = \frac{1}{2\mu} \frac{\partial p}{\partial x} z^2 + Az + B \tag{30}$$

where,

A,B : constants

Applying appropriate boundary conditions Eq. (29) can be solved

$$at\ z = 0 \ \rightarrow u = U_0\ (rotor)$$

$$at\ z = -h(x) \ \rightarrow u = 0\ (stator)$$

Substituting,

$$A = \frac{U_0}{h} + \frac{h}{2\mu} \frac{\partial p}{\partial x}, \qquad B = U_0$$

Therefore velocity can be calculated as:

$$u = \frac{(z^2 - zh)}{2\mu} \frac{\partial p}{\partial x} + \frac{U_0 z}{h} + U_0 \tag{31}$$

Eq. (31) combined with Eq. (1):

$$\tau = \frac{\partial p}{\partial x} \left(z - \frac{h}{2} \right) + \frac{U_0 \mu}{h} \tag{32}$$

The continuity equation for the one-dimensional slider states that:

$$\frac{\partial u}{\partial x}+\frac{\partial w}{\partial z}=0 \tag{33}$$

Integrated Eq. (33) with respect to z we get:

$$w_0^h=\int_0^{-h(x)}\frac{\partial u}{\partial x}dz \tag{34}$$

By substituting Eq. (31) to Eq. (34), interchanging the differentiation and integrating, we get:

$$(w_h-w_0)=-\frac{\partial}{\partial x}\left[\frac{1}{2\mu}\frac{\partial p}{\partial x}\int_0^{-h(x)}(z^2-zh)dz\right]-\frac{\partial}{\partial x}\left[\int_0^{-h(x)}\frac{z}{h}U_0dz\right]=$$
$$-\frac{\partial}{\partial x}\left[\frac{1}{2\mu}\frac{\partial p}{\partial x}\left(\frac{h^3}{3}-\frac{h^2h}{2}\right)\right]-\frac{\partial}{\partial x}\left[\left(\frac{U_0h^2}{2h}\right)\right]=\frac{\partial}{\partial x}\left(\frac{h^3}{12\mu}\frac{\partial p}{\partial x}\right)-\frac{U_0}{2}\frac{\partial h}{\partial x} \tag{35}$$

For steady state conditions $\frac{\partial h}{\partial t}=0$, the left-hand side term $(w_h-w_0)=\frac{\partial h}{\partial t}=0$ so Eq.(35) yields:

$$\frac{\partial}{\partial x}\left(h^3\frac{\partial p}{\partial x}\right)=6\mu U_0\frac{\partial h}{\partial x} \tag{36}$$

Eq. (36) represents the most common form of Reynolds equation. In fixed converging bearings film thickness is a linearly decreasing function of bearing length. To express film thickness we usually use the convergence ratio k (where $k=(h_1-h_0)/h_0$)

h_1, h_0 defined in Figure 6

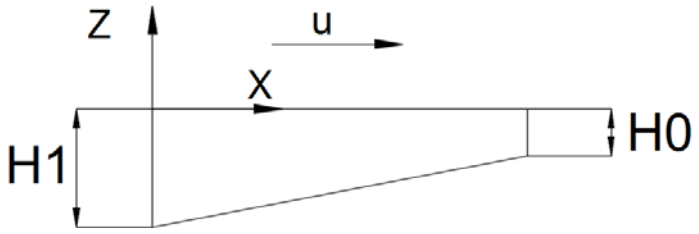

Figure 7 2D sketch of converging wedge and how coordinate system has been taken for calculations

According to Figure 6 h can be calculated as:

$$h=h(x)=h_0+\frac{(h_1-h_0)}{L}\cdot x=h_0\cdot\left(1+\frac{k\cdot x}{L}\right) \tag{37}$$

For a given converging wedge, the pressure distribution over the bearing length can be calculated from the equation:

$$p(x)=\frac{6\mu U_0L}{kh_0}\left(-\frac{1}{h}+\frac{h_0}{h^2}\cdot\frac{k+1}{k+2}+\frac{1}{h_0(k+2)}\right) \tag{38}$$

The lad that a specific film geometry can support is calculated by:

$$W=\int_0^B\int_0^L pdxdy \tag{39}$$

Utilizing the Eq. (38) to Eq. (39) we get:

$$\frac{W}{B} = \frac{6\mu U_0 L}{k^2 h_0^2}\left(-\ln(k+1) + \frac{2k}{k+2}\right) \tag{40}$$

When a thrust bearing operates except for axial (thrust) forces, friction forces arise. Friction forces resist the rotor motion and have a negative impact on the bearings efficiency. The friction force is calculated as the integral of viscous shear stresses over the bearing surface.

$$F = \int_0^B \int_0^L \tau dx \tag{41}$$

The friction per unit width, based on Reynolds theory, can be easily calculated as:

$$\frac{F}{B} = \frac{\mu U_0 L}{h_0}\left(\frac{6}{k+2} - \frac{4\ln(k+1)}{k}\right) \tag{42}$$

Combining Eq. (40) and Eq. (42) friction coefficient, in bearing with infinite width, can be calculated as:

$$f = \frac{F}{W} \xrightarrow{Reynolds} f = \frac{kh_0}{L}\left[\frac{3k-2(k+2)\ln(k+1)}{6k-3(k+2)\ln(k+1)}\right] \tag{43}$$

From Eq. (43) it can be concluded that friction coefficient is independent from viscosity and operational speed. This mean that for a given value of the h_0 term (minimum film thickness), it is possible to optimize performance by finding the optimum value of the convergence ratio.

2.4 Design and performance parameters

Geometry

Trust bearings consist of a different number of pads (usually N_p=6 or 8). A typical arrangement of pad is illustrated in Figure 7. Between its pad there is a groove from where oil is being supplied to each pad. Usually, fresh oil is fed from the inner radius of the pads. Pads principle dimensions (see Figure 8):

- Pad width B
- Inner radius R_{in}
- Outer radius R_{out}
- Pad angle Θ_p
- Groove width L_g
- Pivot radius R_p
- Pivot angle Θ_{pivot}

Figure 8 Typical arrangement of a thrust bearing with eight pads

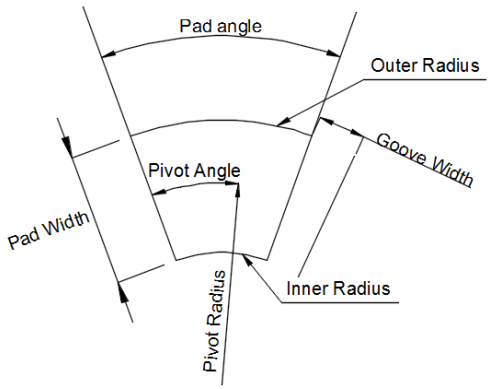

Figure 9 Principal dimensions of a beating pad

The specific pressure that develops in the pad area ranges between 0.5 and 3.0 MPa.

Pivot location

The specific location of the pivot has an important effect on the performance of tilting pad thrust bearings. The pivot location is estimated with the circumferential position

which is expressed as a percentage of pad arc length measured from the inlet face of the pad and his radial position which is determined as percentage of pad width measured from pads inner radius. According to [7] if the pivot is placed between 55 to 58 % of the bearing width the radial tilt angle is zeroed. For the optimal performance of a bearing pivot is placed about 60 % of the pad length, at the circumferential direction, beyond the leading edge. On the other hand, it has been found that a pivot's location at the 70-75 % of the pad length (beyond leading edge) could give the highest possible loads and also the lowest bearing metal temperatures [8]. The simplest, from a manufacturer's point of view, is the centrally located pivot point. According to Reynolds theory, centrally pivot point bearings have zero load carrying capacity due to the asymmetric pressure profile will cause a moment which will align the pad parallel to the collar. A parallel pad is not able to operate because it can't generate hydrodynamic pressure. That, of course, is theoretical because in real operations metals deform, which leads to appropriate wedge film geometries that are able to develop hydrodynamic pressure.

Materials

A quite important parameter, from the manufacturing point of view, is the choice of the bearing material and also their thickness. The maximum pressure that is developed during the operation of a bearing is not large enough to cause damage (Pressure up to 5 MPa). The most crucial thing is to select a material with appropriate thermal properties due to high thermal loads arising from friction. The temperature on stationary pad are higher than those of rotor. This happens mainly because, every point of the pad is exposed to the same flow characteristics unlike to the rotor of which every point periodically passes over cooling grooves that help rotor to reduce its temperature.

Sometimes pads' surface is covered with a thin layer of Babbitt metal. This helps to have better heat conduction. Babbitt metal standout for his resistance to scraping due to its self-lubricating properties. If in any case Babbitt comes in contact with rotor, because Babbitt is quite soft, that prevents from a massive damage of the rotor's surface. Also, in case of any possible damage the replacement of the Babbitt metal is an economic solution.

A new idea that has come into play is to replace Babbitt metal with composite materials. It has been observed that some polymers (PolyTetraFluoroEthylene-PTFE, PelyEtherEtherKetone-PEEK) shows wider temperature ranges, lower friction coefficients and higher resistance against lubrication oil contaminants than metals. In case of the surface of a pad that has covered with PTFE layer has proved to give lower maximum pressure and a more uniform pressure distribution [10]. This mainly came up due to PTFE has lower value of Young's modulus than Babbitt.

Oil properties

The main function of a lubricant is to provide a continuous thin layer between stator and rotor, in order not to come in contact the two parts (for example pad collar), to

prevent wear and reduce friction. Furthermore, oil is being used for heat extraction and from preventing oxidation. The most important property of the lubricant is its viscosity. How much thick will be the thickness of a lubricating film is proportional to its viscosity. This means that lubricant with high values of viscosity can provide thicker films and prevent the two parts to come in contact. However, this doesn't mean that lubricants with the higher value of viscosity are the best for every application. Lubricants with high values of viscosity require more energy levels to flow, thing that increases friction due to generation of heat and also notes an important increase in temperature. In addition, lubricants with high value of viscosity cannot easily penetrate into the hydrodynamic wedge at high speeds. Like in any engineering application the right lubricant has to be properly selected in order to provide optimal performance and make the function of the bearing efficient.

Feeding oil supply rate

There are three requirements that have to be satisfied for the oil feed to the bearing:

i. Sufficient flow into the hydrodynamic wedge (in order to separate the two surfaces)
ii. Additional oil to match the side leakages
iii. Maintain temperatures at the desired levels during the bearing operation.

If a much more oil is supplied to the bearing, due to unnecessary oil stream, a significant amount of churning losses will be developed. An alternative design suggests direct injection of cold and clean lubricant at the entrance of the channel. In that way, there is no mixing of oil that enters with oil that exits, so we don't face phenomena of circulation streams and backflows. The effectiveness of this design is limited in low speed applications.

Rotational speed

Fluid velocity is really important for the functionality of the bearing. At low velocities we have creeping flow so the inertia of the fluid may be ignored. As the fluid velocity is being increased inertia becomes more important and every and each particle of the fluid follows a smooth trajectory and fluid flow is said then to be laminar. Additional increase of fluid's velocity leads to a not desirable flow called "turbulent flow". Turbulent flow may appear into the groove area right next to the pad, but it has been proven experimentally that, for Reynolds number less than 1000, flow in groove area can be considered as laminar [9].

3. Numerical modelling

3.1 Computational fluid dynamics

As mentioned in Chapter 2 the governing equations are solvable only for a small number of flows in fluid mechanics. The solutions are really important to understand fluid flows but they aren't always being used in engineering design or analysis. Engineers in real designs use different approaches for the most of them, with the most widespread being the simplification of the equations that are being used. It is a process that combines approximations and dimensional analysis which represented with non-dimensional parameters such as Reynolds and Froude numbers. With this method researchers reduce the number of independent parameters and are able to perform experiments on scale models by using the condition of geometric similarity. However in many cases it may be impossible to set up a scaled experiment with the most common example of ship. In order to simulate the flow around a ship with his scaled model you have to accomplish the match of Reynolds and Froude numbers which is impossible.

In many cases experiments may be too expensive and time consuming. On the other hand, the measure of some critical data, such as whether fluid separation exists or whether temperature exceed some limits, may be really difficult to obtained. However, with growth of computing abilities in the last century, has come up to a new research field, the Computational Fluid Dynamics (**CFD**). CFD is the new approach between theory and experiments in the field of fluid dynamics. In order to obtain a numerical solution, a discretization method is being used to approximate the differential equations by an algebraic system which will be simple for a computer to solve.

As previously mentioned, CFD methods are simple approximations of complex phenomena. For this reason there are differences between experimental and computed results. This differences are mostly caused due to:

- Errors due to approximations
- Discretization errors
- Errors due to insufficient iterations

3.2 Model definition

In the present study, a three-dimensional thermohydrodynamic (THD) model of tilting pad thrust bearing has been generated, assuming that the collar is rigid and the pad is being deformed with a constant deformation for each case (Normal Load and Double load). Also, the pad has covered with a thin layer of Babbitt. With the CFD code ANSYS CFX, the system of equations presented in Section 3 of Chapter 2 are being solved.

Heat phenomena are taken into account, in particular:

- Rise in temperature caused by viscous flow
- Heat transfer between oil and solids
- Heat exchange with the environment

Geometry

A 3D parametric model of a pivoted pad thrust bearing has been developed using the Autodesk Inventor software. The model consists of a single pad with part of oil and collar above it. Due to, there is no structural link between pad and collar, the load from the rotor is being transferred to the supporting pad through the film of lubricating oil.

The basic geometric parameters of the model according to [2] are presented in the table beneath:

Geometry dimensions	
Number of pads, N_p	8
Outer diameter, D_o	1800 mm
Inner diameter, D_i	800 mm
Pad angle, Θ_p	35 degrees
Pivot circumferential position, Θ_{pivot}	54 % of pad circumferential length
Pivot radius, R_{pivot}	56 % of pad radial width
Pad thickness, t_{pad}	100 mm
Babbitt thickness, $t_{babbitt}$	3 mm
Collar thickness, t_{collar}	80 mm

Table 1 Basic geometry dimensions for the thrust bearing of the present study

Oil and Solid Properties

The thermo-physical properties of the lubricant oil and solids are presented in Table 2.

Lubricant – VG46	
Viscosity law	McCoull and Walther
Dynamic viscosity at 40°C, μ_{40}	0.0398 Pa.s
Dynamic viscosity at 100°C, μ_{100}	0.0060 Pa.s
Density, ρ	867 kg/m^3
Thermal conductivity, λ_f	0.13 W/m.K
Heat Capacity, c_{pf}	2035 J/kg.K
Oil temperature at inlet point, T_{in}	30°C
Feeding oil flow rate, Q_{feed}	0.00017 m^3/s
Collar - Pad	
Thermal conductivity, λ_s	47 W/m.K
Heat capacity, c_{ps}	434 J/kg.K
Babbitt	
Thermal conductivity, λ_b	24 W/m.K
Heat capacity, c_{pb}	230 J/kg.K

Table 2 Thermophysical properties of the lubricant oil and solids

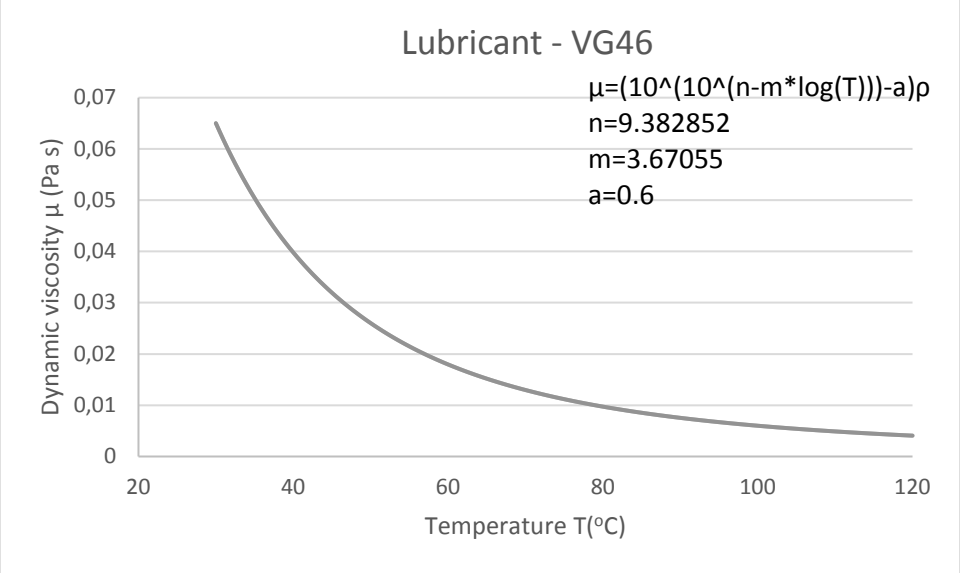

Figure 10 Temperature dependence of VG46 viscosity

Boundary Conditions

Boundary conditions shows how the flow conditions has been defined at each face of the domain. Every domain consist of 6 faces. In the present study boundary conditions has been taken as shown in the Table 3.

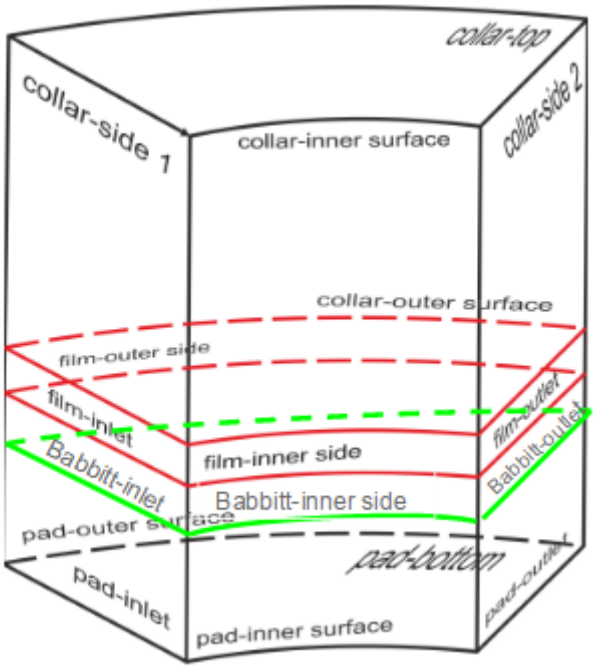

Figure 11 Sector pad bearing: name convention of rotor, pad, Babbitt and film boundary surfaces

Collar	
Top surface / Outer surface	Heat transfer coeff: 25 $W/m^2.K$, $T_{amb}=20^oC$
Bottom	Fluid-Solid interface: Continuity of heat flux and temperature
Inner surface	Heat transfer coeff: 1000 $W/m^2.K$,T_{amb} =30^oC
Sides	Periodic Conditions
Pad	
Top	Solid-Solid interface: Continuity of heat flux and temperature
Bottom / Outer surface / Inner surface	Heat transfer coeff: 100 $W/m^2.K$, $T_{amb}=30^oC$
Inlet Side / Outlet Side	Heat transfer coeff: 100 $W/m^2.K$, $T_{amb}=30^oC$
Fluid Domain	
Inlet	Opening: zero relative pressure*, Opening Temp.=30^oC
Outer side / Outlet	Outlet: zero relative pressure*,
(*) n is the vector normal to the surface	
Babbitt	
Inlet / Inner / Outer side / Outlet	Heat transfer coeff: 100 $W/m^2.K$, $T_{amb}=30^oC$
Bottom	Solid-Solid interface: Continuity of heat flux and temperature
Top	Fluid-Solid interface: Continuity of heat flux and temperature

Table 3 Thermal and flow boundary conditions of the model

3.3 The Newton – Raphson method

In order to adjust the film geometry there has been built a code of Newton-Raphson method which takes the parameters of h_{pivot}, θ_{pitch}, θ_{roll} and adjust them according to the equations below:

$$W - W_{req} = \int_0^L \int_0^B p_{HS} dxdy - W_{req} = 0 \quad (44)$$

$$M_{x,p} = \int_0^L \int_0^B p_{HS} x dxdy = 0 \quad (45)$$

$$M_{y,p} = \int_0^L \int_0^B p_{HS} y dxdy = 0 \quad (46)$$

p_{HS}: pressure after application of the Half-Sommerfeld boundary condition

$$p_{HS} = \begin{Bmatrix} p \text{ if } p \geq 0 \\ 0 \text{ if } p < 0 \end{Bmatrix}$$

If Eq. (44) - (46) are below a threshold means that we have reach the desired film geometry.

The Newton-Raphson method is a simple multidimensional root-finding technique which can be applied to any N-dimensional system. Starting with an initial guess for the independent variables, the main idea of the Newton-Raphson method is that a function is approximated locally by its tangent line. The point of intersection between the tangent line and the x-axis will be a better approximation of the function's root than the first guess and the method continues that way until it reaches to a solution.

In our case we have a system of three functional relations to be zeroed with three independent variables:

$$F_1(x_1, x_2, x_3) = 0 \quad (47)$$

$$F_2(x_1, x_2, x_3) = 0 \quad (48)$$

$$F_3(x_1, x_2, x_3) = 0 \quad (49)$$

Newton-Raphson's method requires the calculation of the functions derivatives. The approximation of the true local derivatives, if the analytical expressions aren't available are defined as:

$$F'(x) \approx \frac{F(x+dx)-F(x)}{dx} \quad (50)$$

In the neighborhood of x, each of the functions F_i can be expanded in Taylor series:

$$F_i(x + \delta x) = F_i(x) + \sum_{j=1}^{3} \frac{\partial F_i}{\partial x_j} \delta x_j + o(\delta x^2) \quad i = (1,2,3)\ j = (1,2,3) \quad (51)$$

The matrix of partial derivatives appearing in Eq. (51) is the Jacobian matrix *J*:

$$J = \begin{bmatrix} \frac{\partial F_1}{\partial x_1} & \frac{\partial F_1}{\partial x_2} & \frac{\partial F_1}{\partial x_3} \\ \frac{\partial F_2}{\partial x_1} & \frac{\partial F_2}{\partial x_2} & \frac{\partial F_2}{\partial x_3} \\ \frac{\partial F_3}{\partial x_1} & \frac{\partial F_3}{\partial x_2} & \frac{\partial F_3}{\partial x_3} \end{bmatrix} \quad (52)$$

The determinant of matrix *J* is calculated:

$$detJ = \frac{\partial F_1}{\partial x_1}\left(\frac{\partial F_2}{\partial x_2}\cdot\frac{\partial F_3}{\partial x_3} - \frac{\partial F_2}{\partial x_3}\cdot\frac{\partial F_3}{\partial x_2}\right) - \frac{\partial F_1}{\partial x_2}\left(\frac{\partial F_2}{\partial x_1}\cdot\frac{\partial F_3}{\partial x_3} - \frac{\partial F_3}{\partial x_1}\cdot\frac{\partial F_2}{\partial x_3}\right) + \frac{\partial F_1}{\partial x_3}\left(\frac{\partial F_2}{\partial x_1}\cdot\frac{\partial F_3}{\partial x_2} - \frac{\partial F_3}{\partial x_1}\cdot\frac{\partial F_2}{\partial x_2}\right) \quad (53)$$

By neglecting terms of order δx^2 and higher and also by setting $F_i(x+\delta x) = 0$, we obtain a set of linear equations for the corrections δx that move each function closer to zero simultaneously, namely:

$$J \cdot \delta x = -F \quad (54)$$

The corrections are then added to the solution vector:

$$x_{new} = x_{old} + \delta x \quad (55)$$

Which, in expanded form, reads:

$$x_{1,new} = x_{1,old} - \left(\left(\frac{\partial F_2}{\partial x_2}\cdot\frac{\partial F_3}{\partial x_3} - \frac{\partial F_2}{\partial x_3}\cdot\frac{\partial F_3}{\partial x_2}\right)\cdot F_1(x_{1,old}) + \left(\frac{\partial F_1}{\partial x_3}\cdot\frac{\partial F_3}{\partial x_2} - \frac{\partial F_3}{\partial x_3}\cdot\frac{\partial F_1}{\partial x_2}\right)\cdot F_2(x_{1,old}) + \left(\frac{\partial F_2}{\partial x_3}\cdot\frac{\partial F_2}{\partial x_3} - \frac{\partial F_1}{\partial x_3}\cdot\frac{\partial F_2}{\partial x_2}\right)\cdot F_3(x_{1,old})\right)/detJ \quad (56)$$

$$x_{2,new} = x_{2,old} - \left(\left(\frac{\partial F_2}{\partial x_3}\cdot\frac{\partial F_3}{\partial x_1} - \frac{\partial F_3}{\partial x_3}\cdot\frac{\partial F_2}{\partial x_1}\right)\cdot F_1(x_{2,old}) + \left(\frac{\partial F_1}{\partial x_1}\cdot\frac{\partial F_3}{\partial x_3} - \frac{\partial F_1}{\partial x_3}\cdot\frac{\partial F_2}{\partial x_1}\right)\cdot F_2(x_{2,old}) + \left(\frac{\partial F_1}{\partial x_3}\cdot\frac{\partial F_2}{\partial x_1} - \frac{\partial F_2}{\partial x_3}\cdot\frac{\partial F_1}{\partial x_1}\right)\cdot F_3(x_{2,old})\right)/detJ \quad (57)$$

$$x_{3,new} = x_{3,old} - \left(\left(\frac{\partial F_2}{\partial x_1}\cdot\frac{\partial F_3}{\partial x_2} - \frac{\partial F_2}{\partial x_2}\cdot\frac{\partial F_3}{\partial x_1}\right)\cdot F_1(x_{3,old}) + \left(\frac{\partial F_1}{\partial x_2}\cdot\frac{\partial F_3}{\partial x_1} - \frac{\partial F_3}{\partial x_2}\cdot\frac{\partial F_1}{\partial x_1}\right)\cdot F_2(x_{3,old}) + \left(\frac{\partial F_1}{\partial x_1}\cdot\frac{\partial F_2}{\partial x_2} - \frac{\partial F_1}{\partial x_2}\cdot\frac{\partial F_2}{\partial x_1}\right)\cdot F_3(x_{3,old})\right)/detJ \quad (58)$$

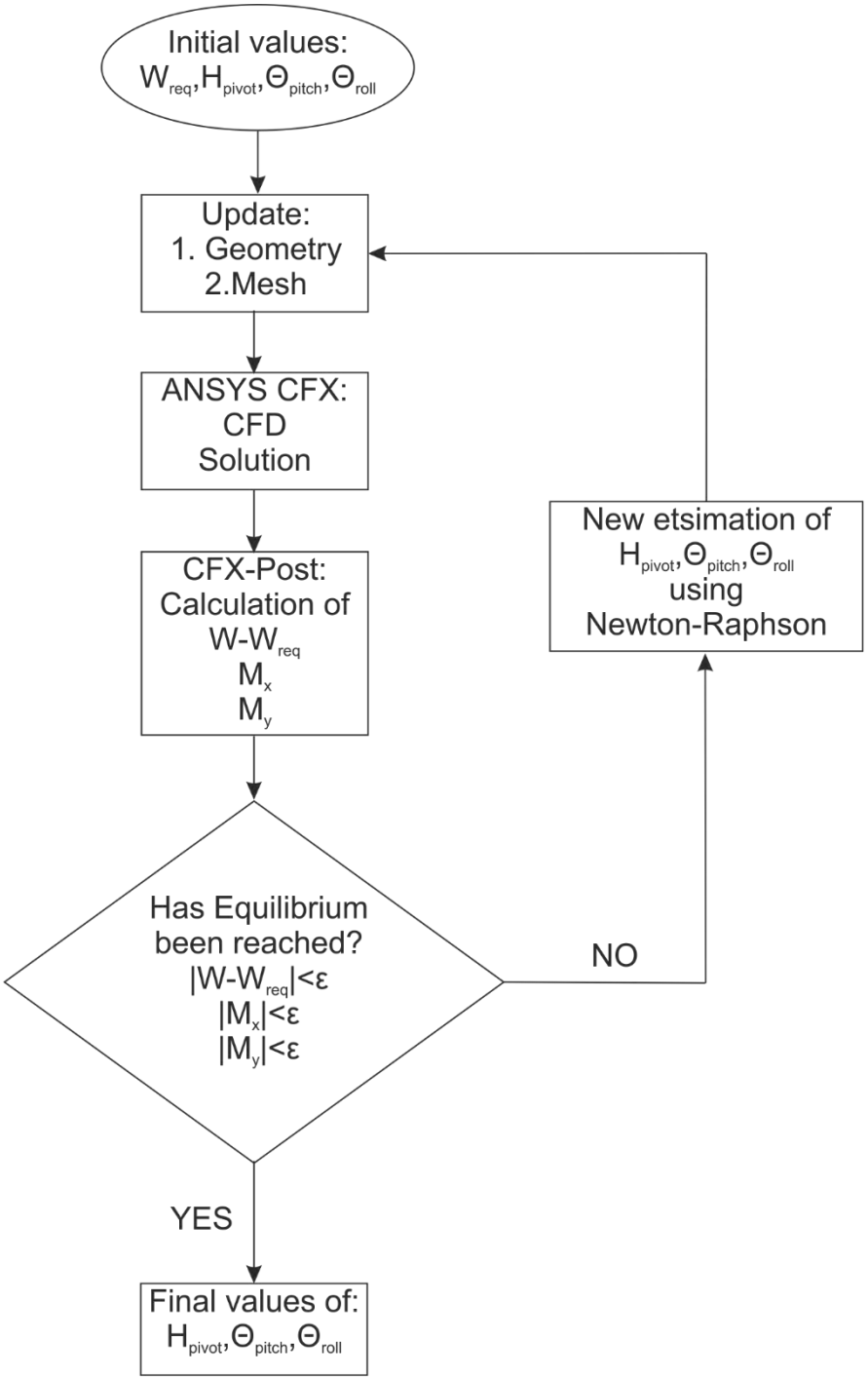

Figure 12 Schematic process of Newton-Raphson method

3.4 Mesh study

The equations showed in Section 2.3 are solvable for a finite volume grid. The main purpose is to discretize, a large continuous physical domain, in small pieces for which the solution of complex equations will be feasible. An important factor is the quality and density of the mesh that will be used. A quite fine grid can lead to better and more realistic results and find a solution faster, but it may burden the performance of the software.

In the present model, we used a hexahedral mesh for all domains (pad, Babbitt, collar, film). In order to approach the thermal boundary layer with good accuracy, we made a denser grid to the rigid surfaces. In the Figure 12 a typical mesh o our model is depicted.

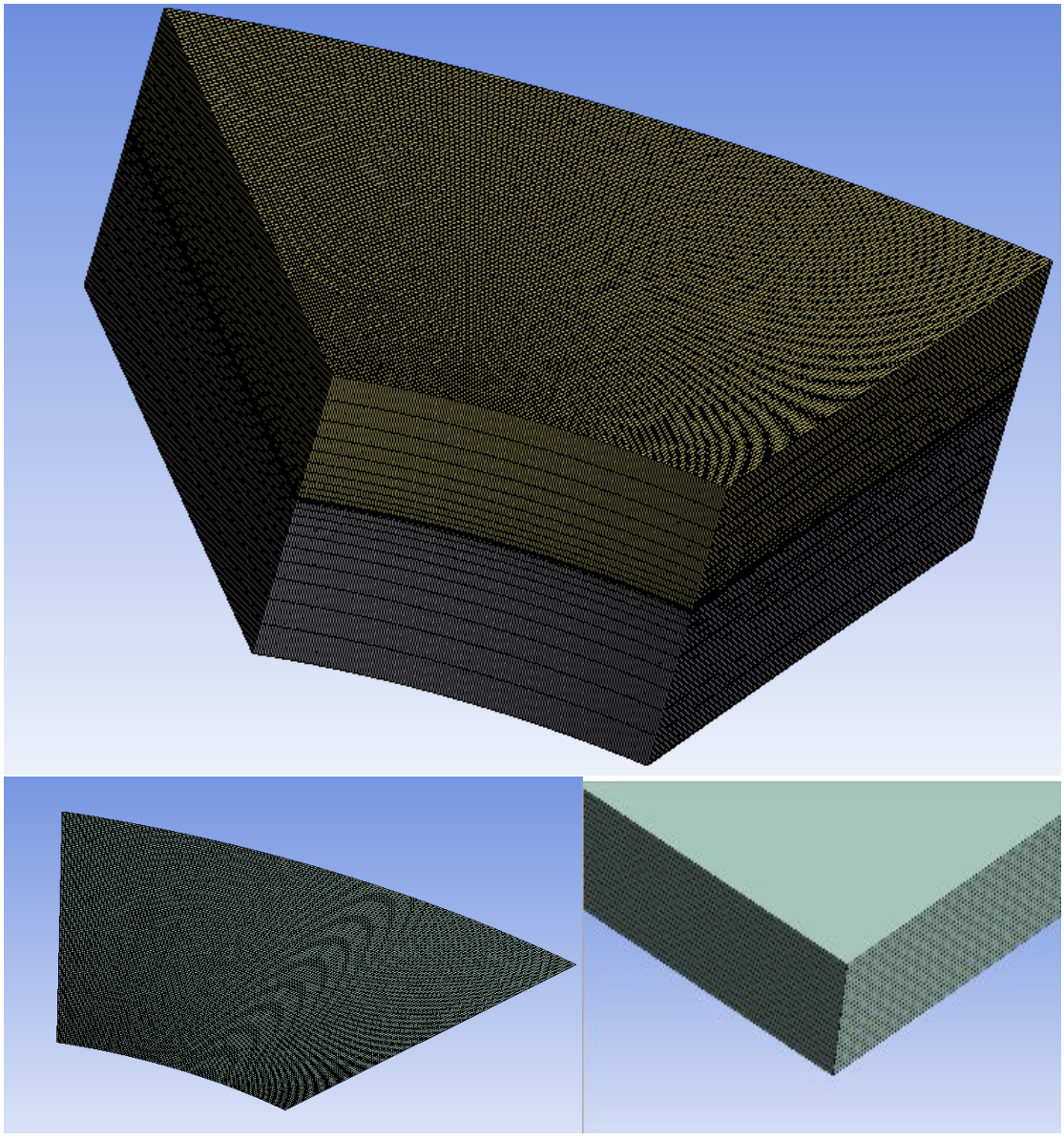

Figure 13 Typical mesh of model of the present study

A mesh study was performed in order to verify the accuracy of the results given by the different grids. We changed the element layers along the film thickness and the number of divisions across the two different directions (radially and circumferentially). We tested the mesh quality at the design case of 187.5 RPM and at load capacity of 680 kN. The results are given in the Figure 13.

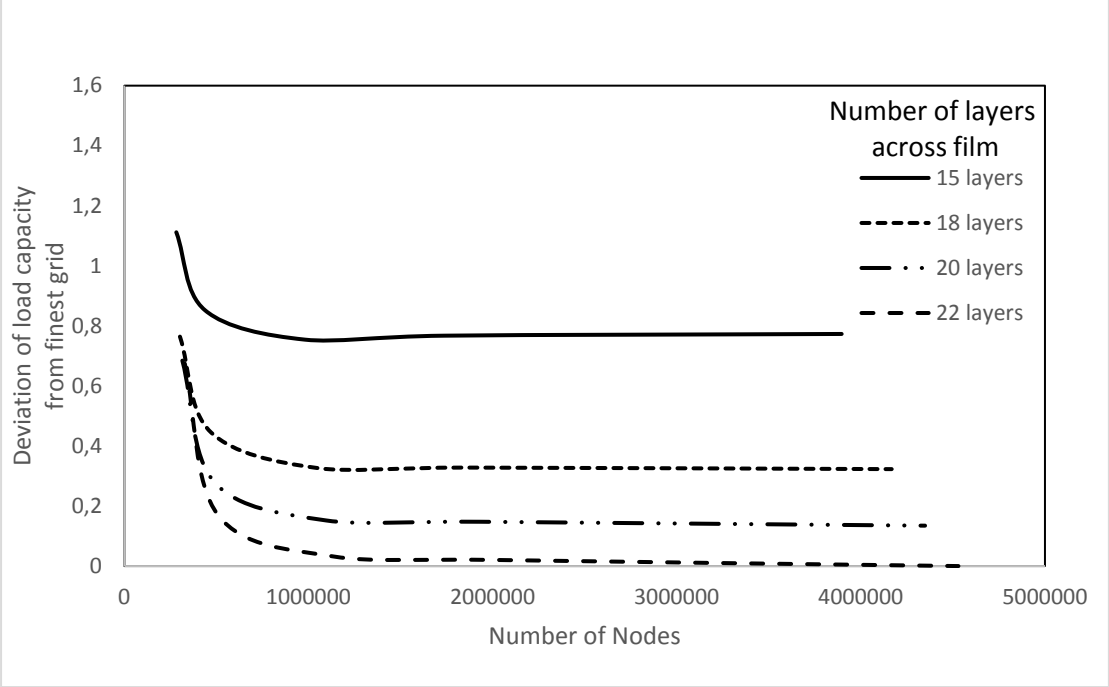

Figure 14 Mesh study analysis

As can been seen, if number of layers are greater than 18 layers along film thickness and number of nodes greater than 1 million, the deviation of load capacity from finest grid is lower than 0.4 %. In our cases it was chosen the grid with 22 layers along film thickness and 150 number of divisions across the two different directions (approximately 1 million of nodes). Even though it was too dense for the simple case of the deformed pad we took it to be sure that it will provide sufficient accuracy for the cases examined in Chapter 4.

4. Thrust Bearing Simulations

In the present study, a model of single pad with the included oil film and part of rotor above it has been studied, under the effect of two different thrust loads:

i. 680 kN
ii. 1360 kN

For each load we compare the results of the basic model, which is the state of deformed pad model, with the cases of concavity, convexity, one-sinewave, three-sinewaves and five-sinewaves (we assume that error amplitudes are functions of sinewaves). Every case has been examined for error amplitudes from zero (deformed model) to twenty microns. At the end, we will be able to see how the manufacturing errors affect the functionality of the thrust bearing.

4.1 Thrust load of 680 kN

4.1.1 Deformed pad geometry

In the deformed state of the pad we have assumed a constant deformation of **20 microns** from plain pad across the two directions (radially, circumferentially) with this value stated at the inner radius (radially) and the intake of the oil film. This assumption has been taken from the TEHD study [2]. The deformation of the pad has been simulated as a parabola with its center at the pivot position of the pad. A typical 3D sketch of deformed pad situation is depicted in Figure 14, in enlargement.

(a) **(b)**

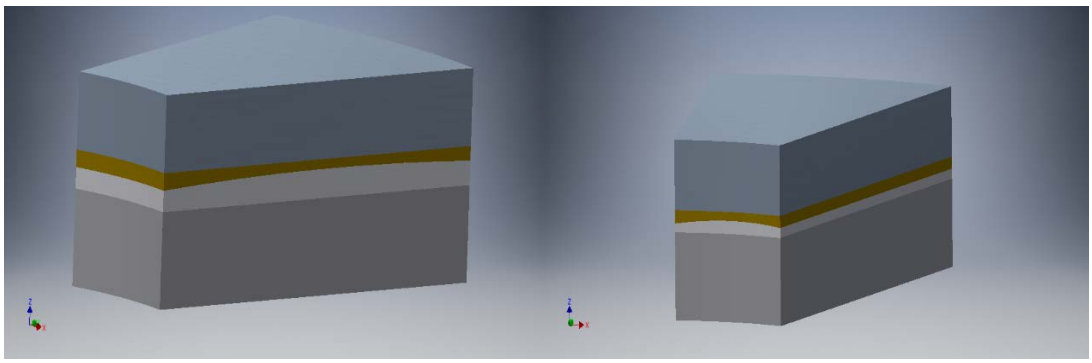

Figure 15 (a) Pad deformed radially, (b) Pad deformed circumferentially

In Figure 15, it is showed how the temperature of the model is being formed and also how heat power is being transferred through the solid parts.

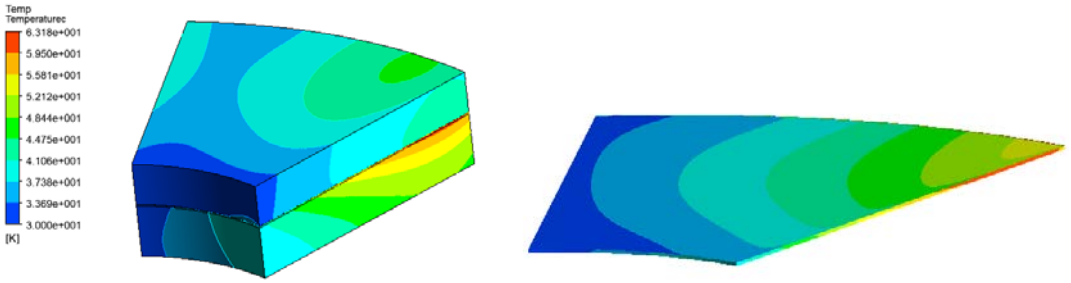

Figure 16 Temperature distribution in the lubricant and solid domains of the bearing pad.

Figure 16 (a) presents the distribution of pressure at three different positions (25% pad width, 50% pad width and 75% pad width). As shown, the biggest pressure appears at the mid sector and as we get away from the mid sector the pressure decreases, mostly due to fluid leakage. Figure 16 (b) presents the distribution of temperature at the same position. In temperatures situation we see that the max temperature increases as we reach at the outer point of the pad and maximizes at the position where the H_{min} point reach (see contour of temperature). Figure 16 (c) shows the film region between pad and collar.

(a)

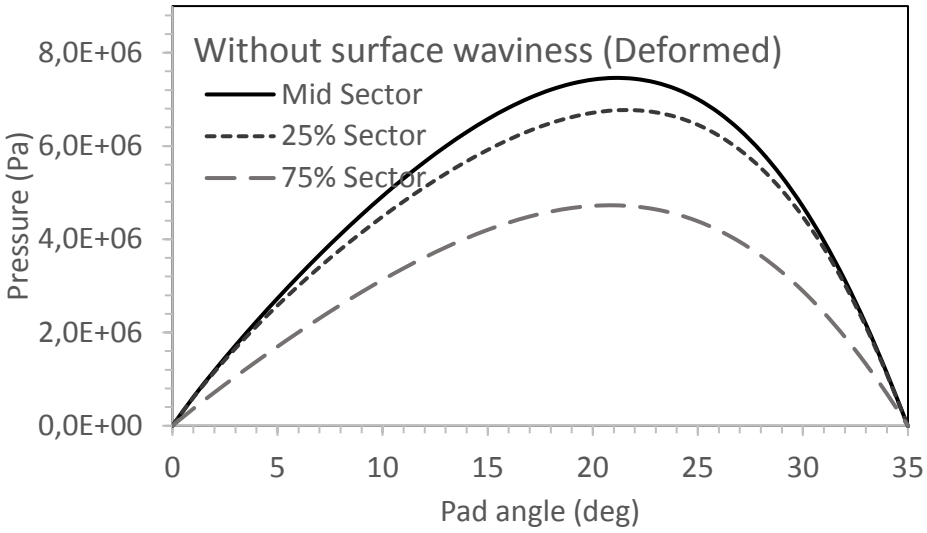

(b)

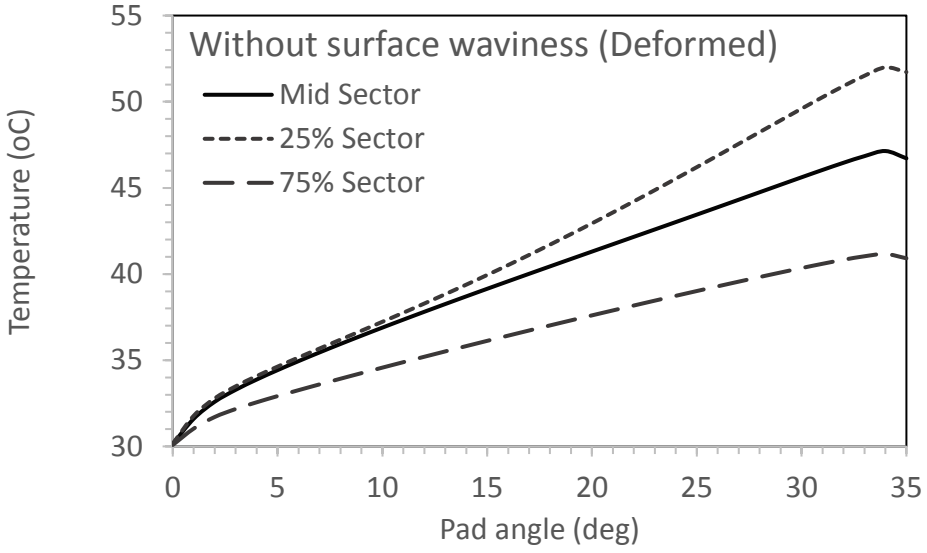

(c)

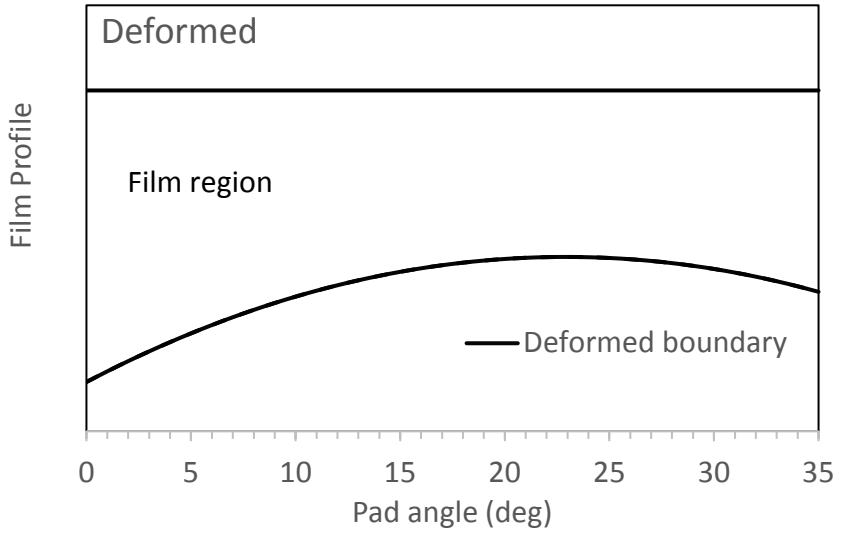

Figure 17 Deformed: (a)Chart of pressure (b)Chart of temperature (c)Film Profile

In Figure 17, contour of pressure, temperature and film thickness are presented. Temperature attains a maximum at the outer region of the bearing close to the lubricant outflow. This can be attributed to the effect that collar and pad are at the closest distance and oil heating due to viscous dissipation as well as the action of centrifugal forces. Pressure is being maximized at approximately of 65% percent of the bearing min sector (from inlet point). Minimum film thickness appears at back outflow position of pad as seen in picture below.

(a) **(b)** **(c)**

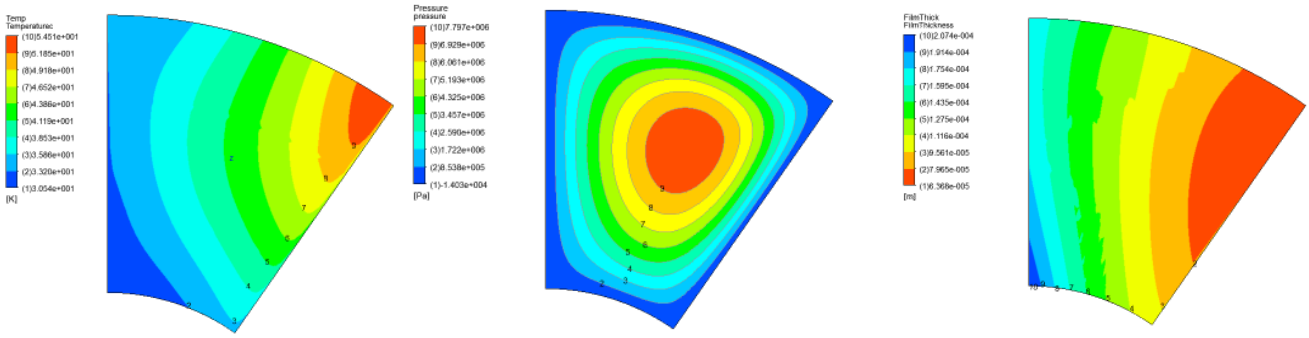

Figure 18 Contours of deformed pad : (a), (b) Temperature / pressure distribution at the babbitt-film interface, and (c)Film thickness distribution.

4.1.2 Convexity

In case of convexity, as Figure 18 presents, minimum Film thickness increases up to 6.5%. The friction torque decreases 0.8% and as a consequence, temperature decreases 1.5^{o}C.

(a)

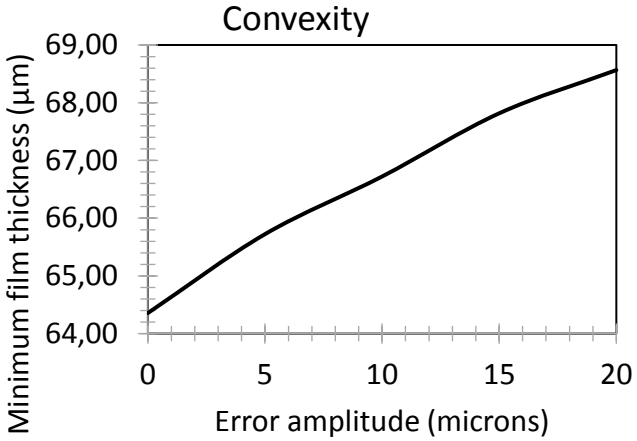

(b)

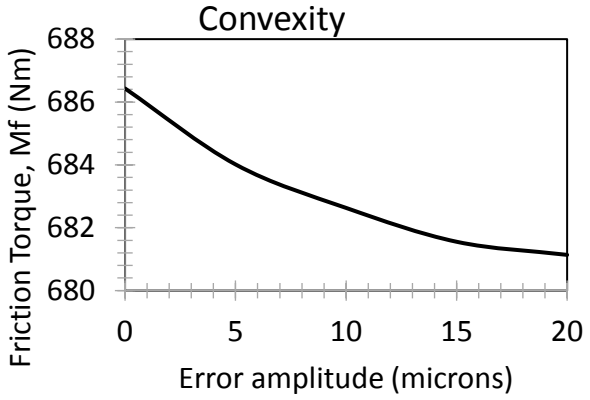

(c)

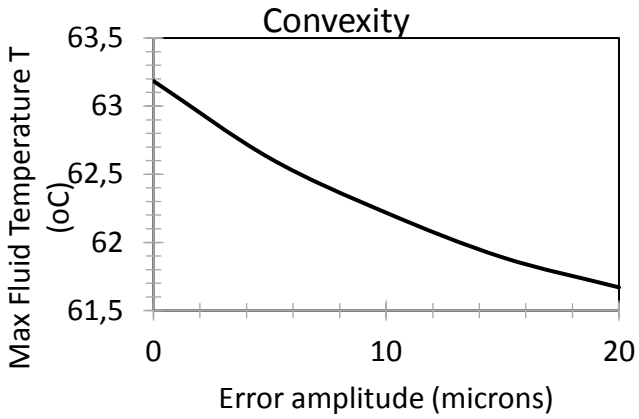

Figure 19 Performance of thrust bearing with manufacturing error "convexity" compared to the deformed bearing (a) Minimum film thickness (b) Friction torque (c) Max fluid temperature

Subsequently, the chart of pressure and temperature and film profile is being presented in Figure 19.

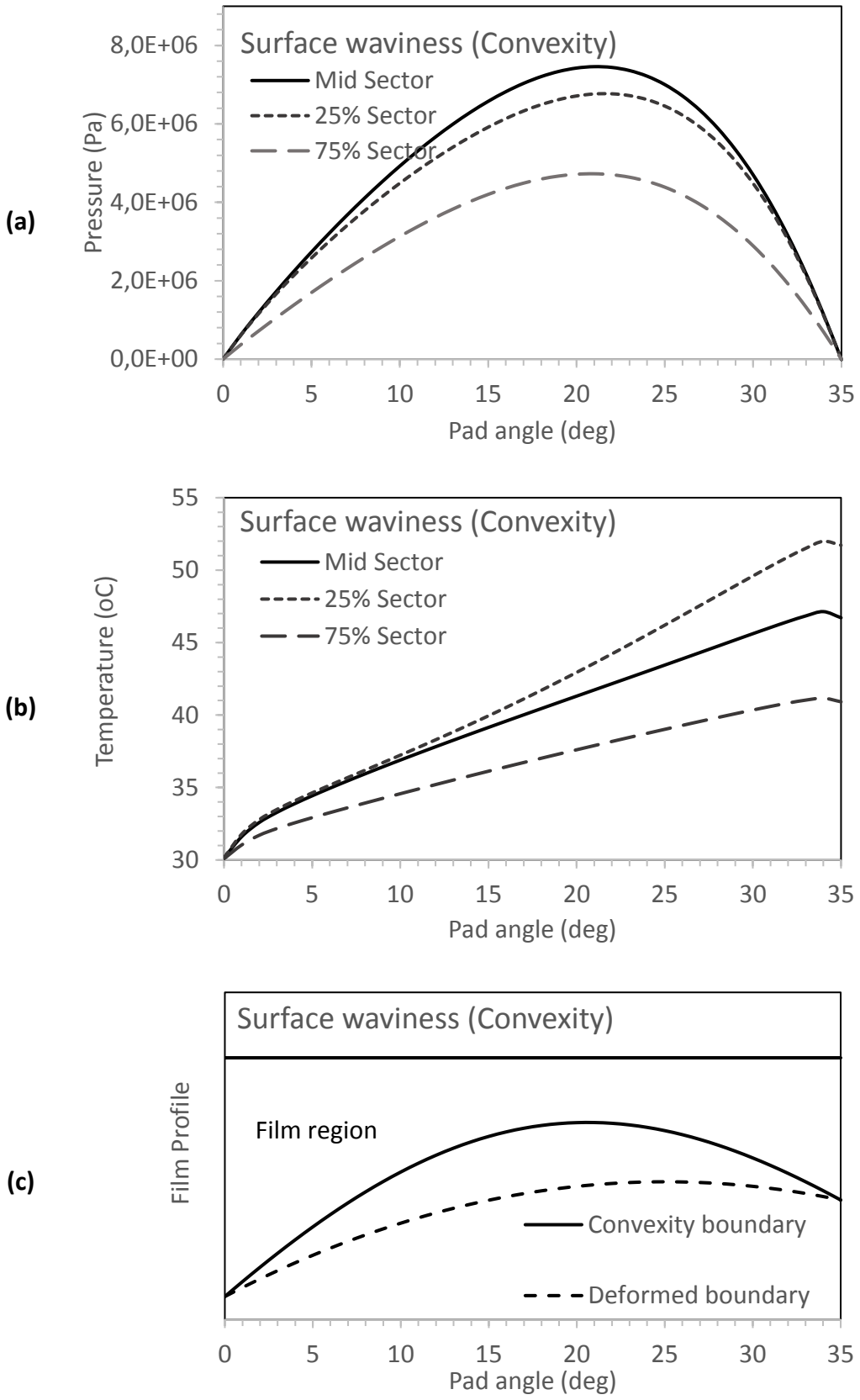

Figure 20 Convexity manufacturing error: (a) Pressure distributions, (b) Temperature distributions, and (c) Film profile

At the end, the contours of temperature, pressure and film thickness is being presented for the case of manufacturing errors with amplitude 20 microns.

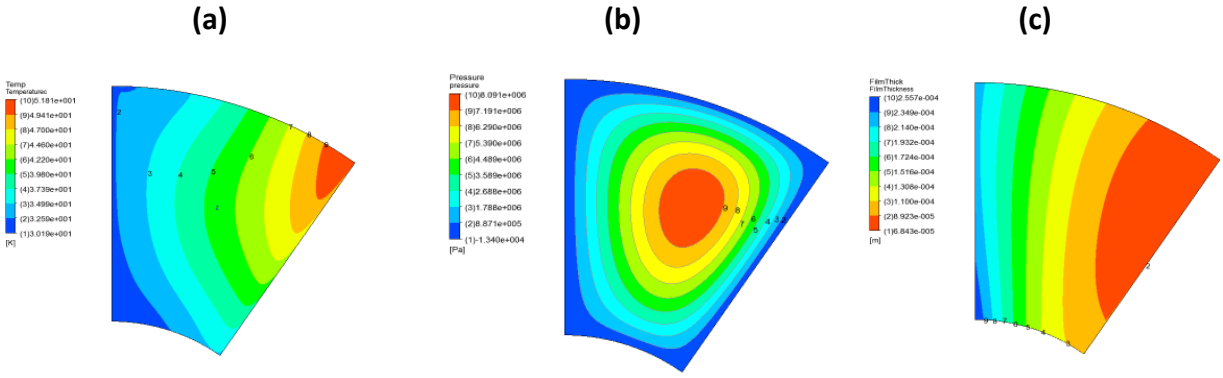

Figure 21 Contours of convexity: (a), (b) Temperature / pressure distribution at the babbitt-film interface, and (c)Film thickness distribution.

4.1.3 Concavity

Concavity affects the performance of thrust bearing as: Minimum film thickness decreases 23.9%, friction torque increases 4.8% and temperature also increases 10.8^{o}C.

(a)

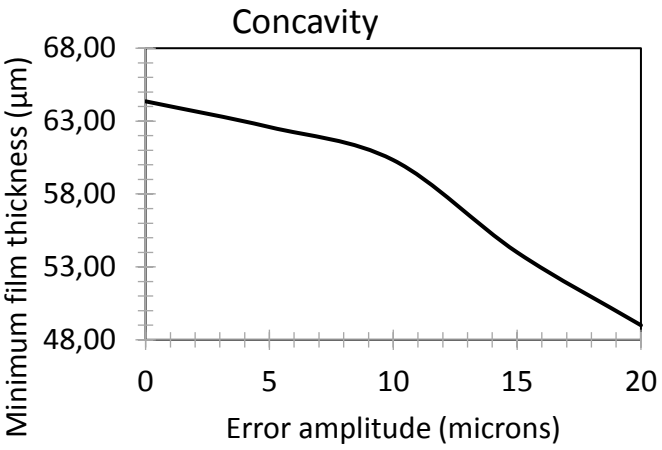

(b)

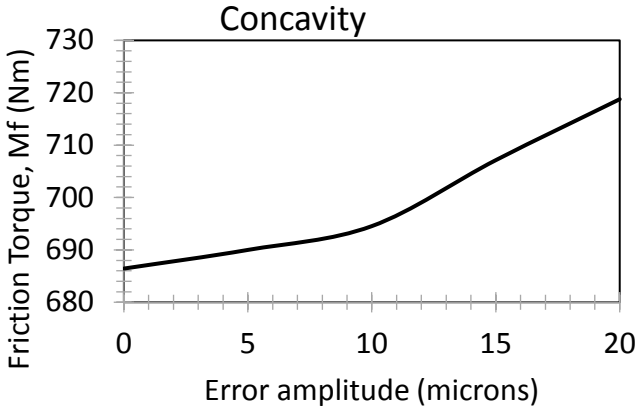

(c)

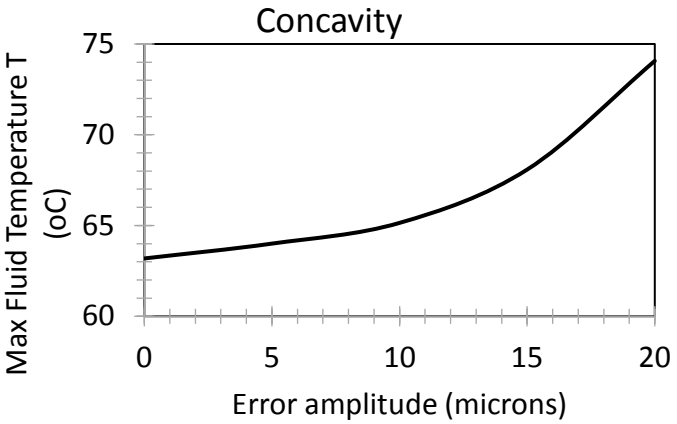

Figure 22 Performance of thrust bearing with manufacturing error "concavity" compared to the deformed bearing (a) Minimum film thickness (b) Friction torque (c) Max fluid temperature

Figure 22 presents the charts of pressure and temperature and film profile.

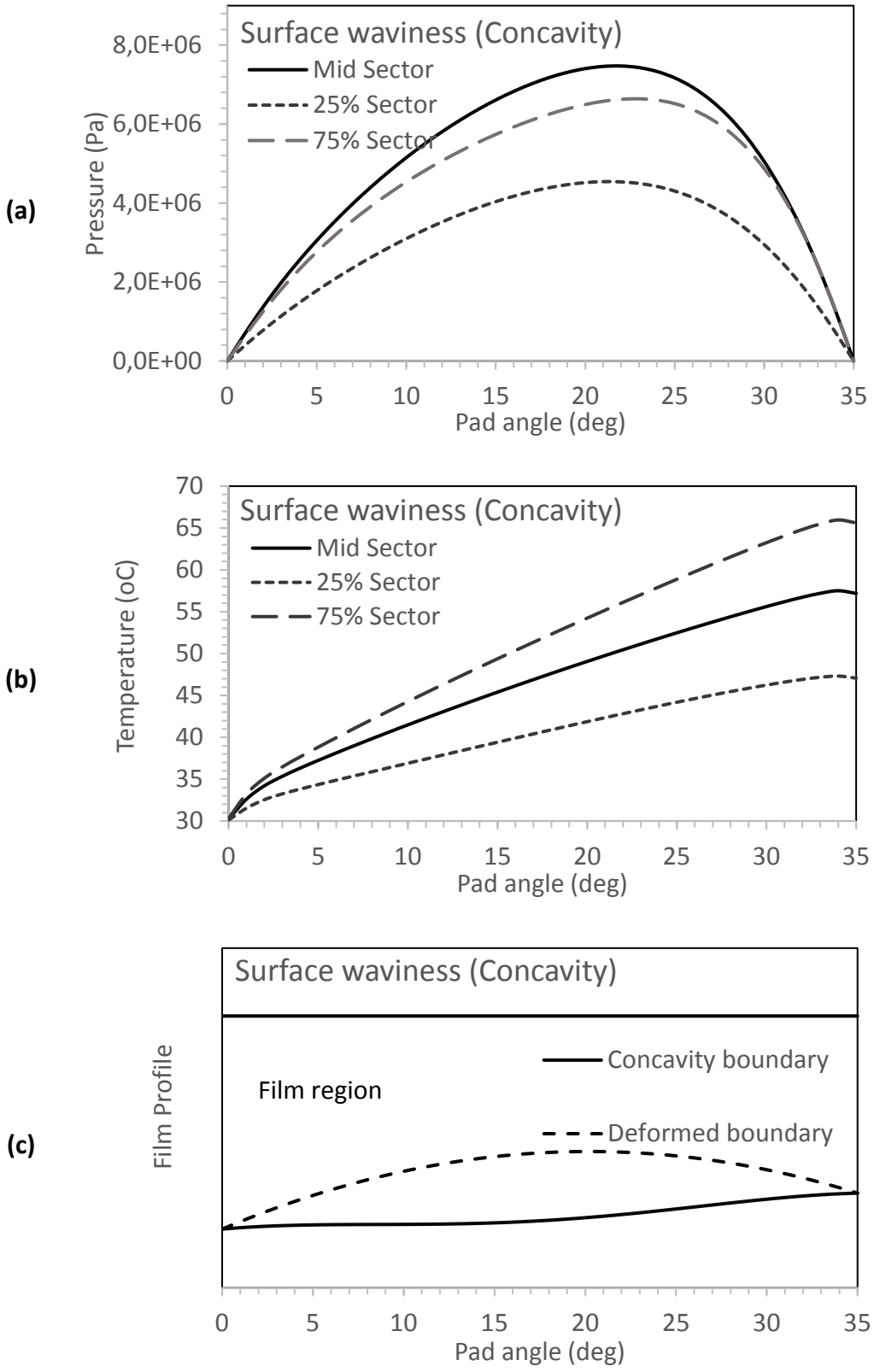

Figure 23 Concavity manufacturing error: (a) Pressure distributions, (b) Temperature distributions, and (c) Film profile

Finally, the contours of temperature, pressure and film thickness is being presented for the case of manufacturing errors with amplitude 20 microns.

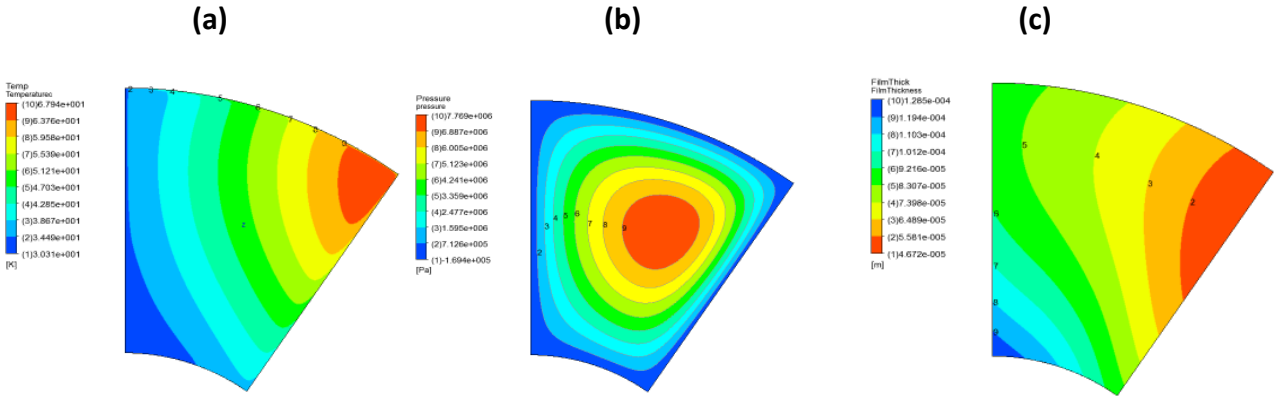

Figure 24 Contours of concavity: (a), (b) Temperature / pressure distribution at the babbitt-film interface, and (c) Film thickness distribution.

4.1.4 Waviness error - one sinewave

The influence of one sinewave on the performance of thrust bearings is: Minimum film thickness can increase by up to 8.8%, friction torque decreases by up to 0.4% and temperature decreases by up to 2.1^{o}C.

(a)

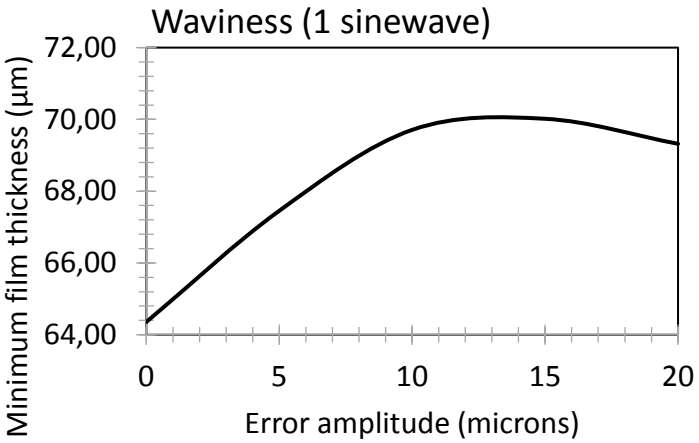

(b)

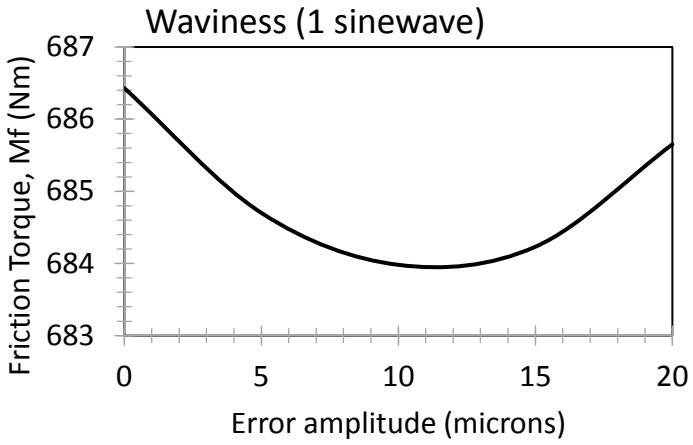

(c)

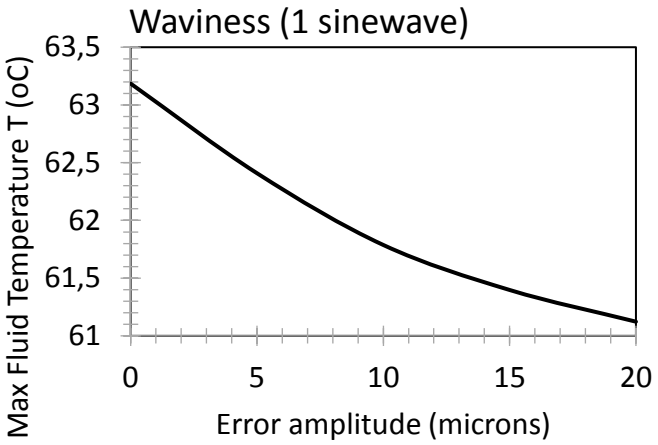

Figure 25 Performance of thrust bearing with manufacturing error "one sinewave" compared to the deformed bearing (a) Minimum film thickness (b) Friction torque (c) Max fluid temperature

In the Figure below, we see the pressure and temperature charts.

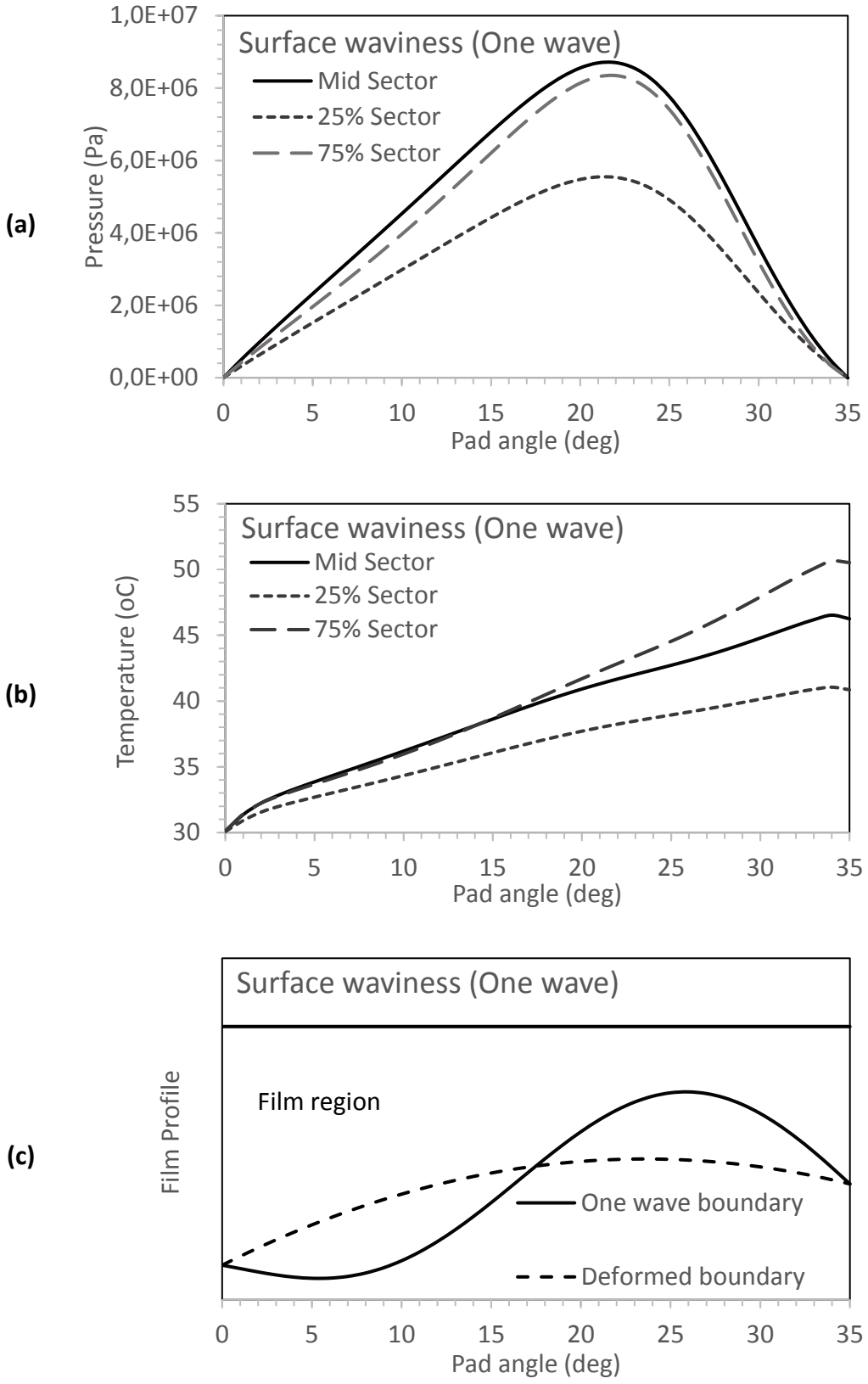

Figure 26 One sinewave manufacturing error: (a) Pressure distributions, (b) Temperature distributions, and (c) Film profile

Figure 26 presents the contours of temperature, pressure and film thickness for the case of manufacturing errors with amplitude 20 microns

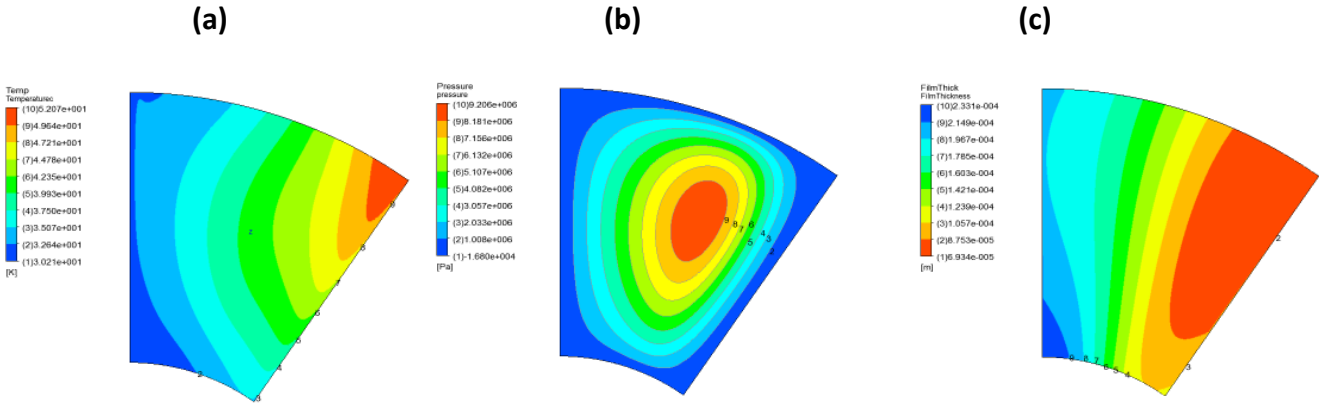

Figure 27 Contours of one sinewave: (a), (b) Temperature / pressure distribution at the babbitt-film interface, and (c) Film thickness distribution.

4.1.5 Waviness error – three sinewaves

The existence of three sinewaves affect the performance of thrust bearing as follows: Minimum film thickness decreases 14.8%, friction torque increases 2.4% and temperature also increases by 1.7^{o}C.

(a)

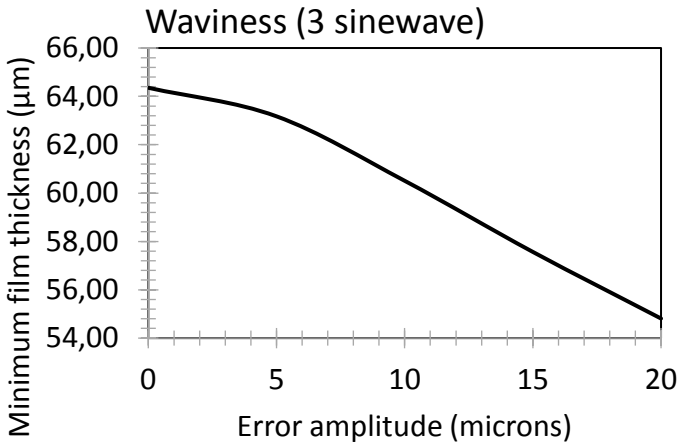

(b)

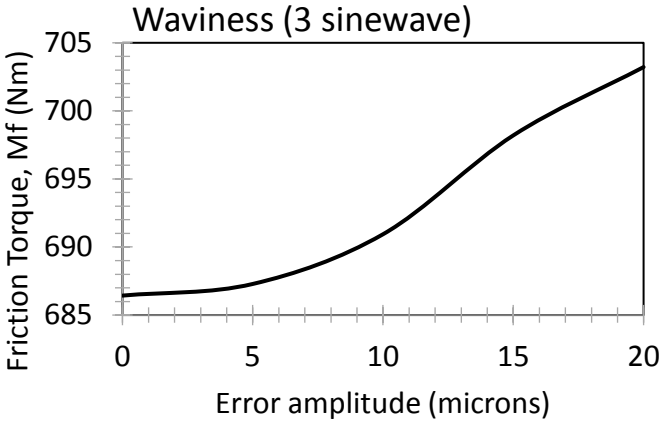

(c)

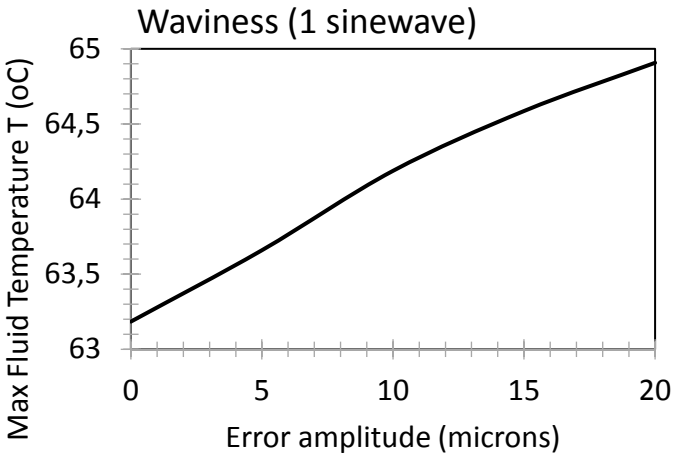

Figure 28 Performance of thrust bearing with manufacturing error "three sinewave" compared to the deformed bearing (a) Minimum film thickness (b) Friction torque (c) Max fluid temperature

Figure 28 shows the pressure temperature and film profile charts. From the charts we can clearly see the significant influence of the waves from the fluctuation in pressure profile. The impact in temperature profile due to waviness is negligible.

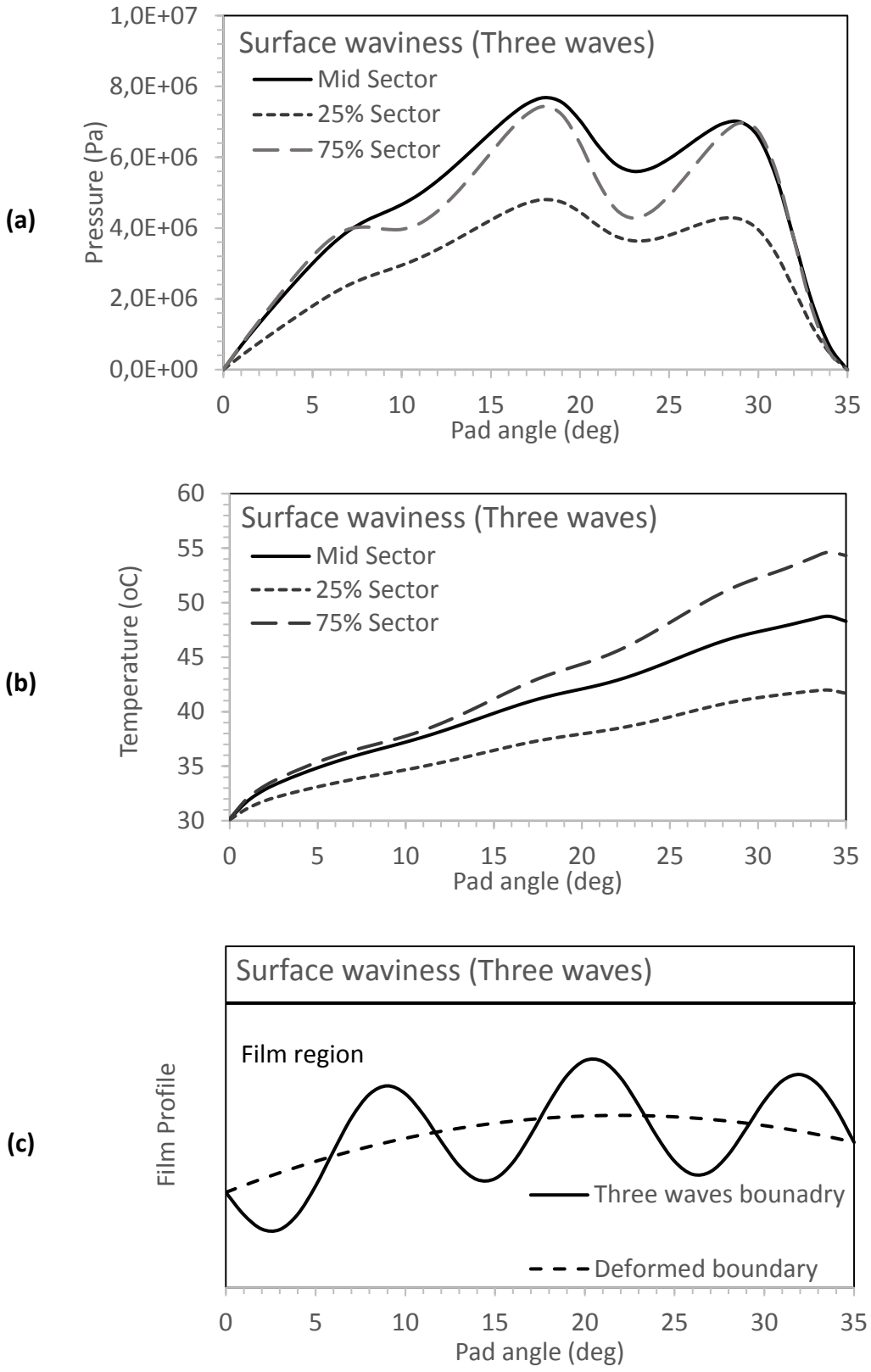

Figure 29 Three sinewave manufacturing error: (a) Pressure distributions, (b) Temperature distributions, and (c) Film profile

Finally, the contours of temperature, pressure and film thickness is being presented for the case of manufacturing errors with amplitude 20 microns.

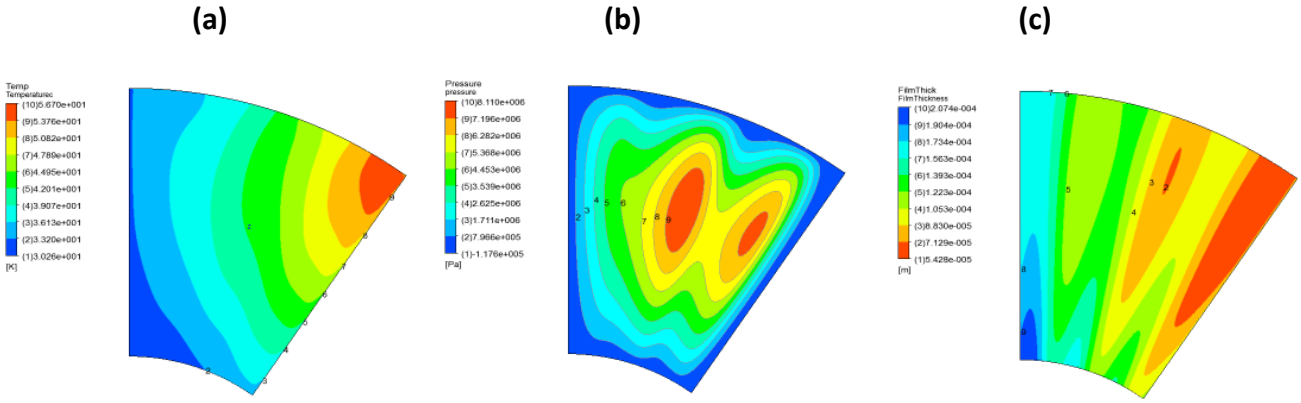

Figure 30 Contours of three sinewave: (a), (b) Temperature / pressure distribution at the babbitt-film interface, and (c) Film thickness distribution.

4.1.6 Waviness error – five sinewaves

The influence of five sinewaves in the performance of thrust bearing is as follows: Minimum film thickness decreases by 18.2%, friction torque increases by 1.9% and temperature also increases by 1.6^{o}C.

(a)

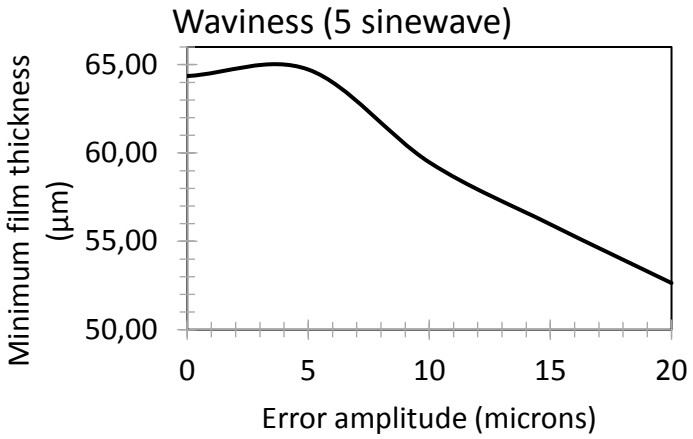

(b)

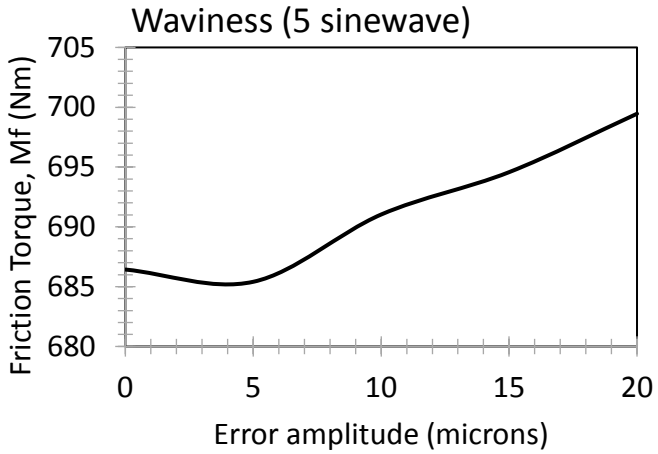

(c)

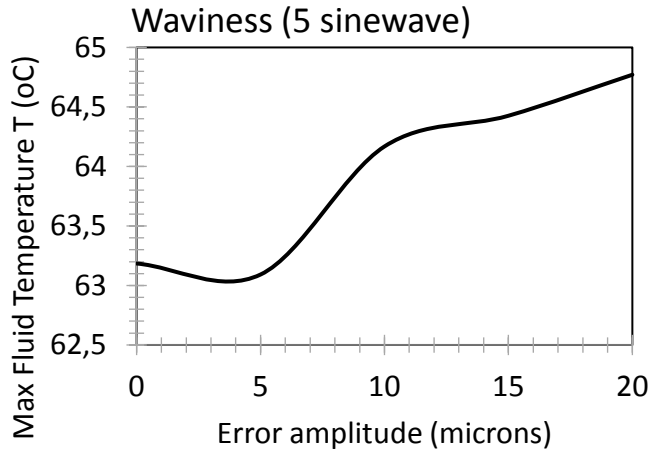

Figure 31 Performance of thrust bearing with manufacturing error "five sinewave" compared to the deformed bearing (a) Minimum film thickness (b) Friction torque (c) Max fluid temperature

In Figure 31 we see the pressure and temperature charts. As in case of three sinewaves the influence of waviness is the same.

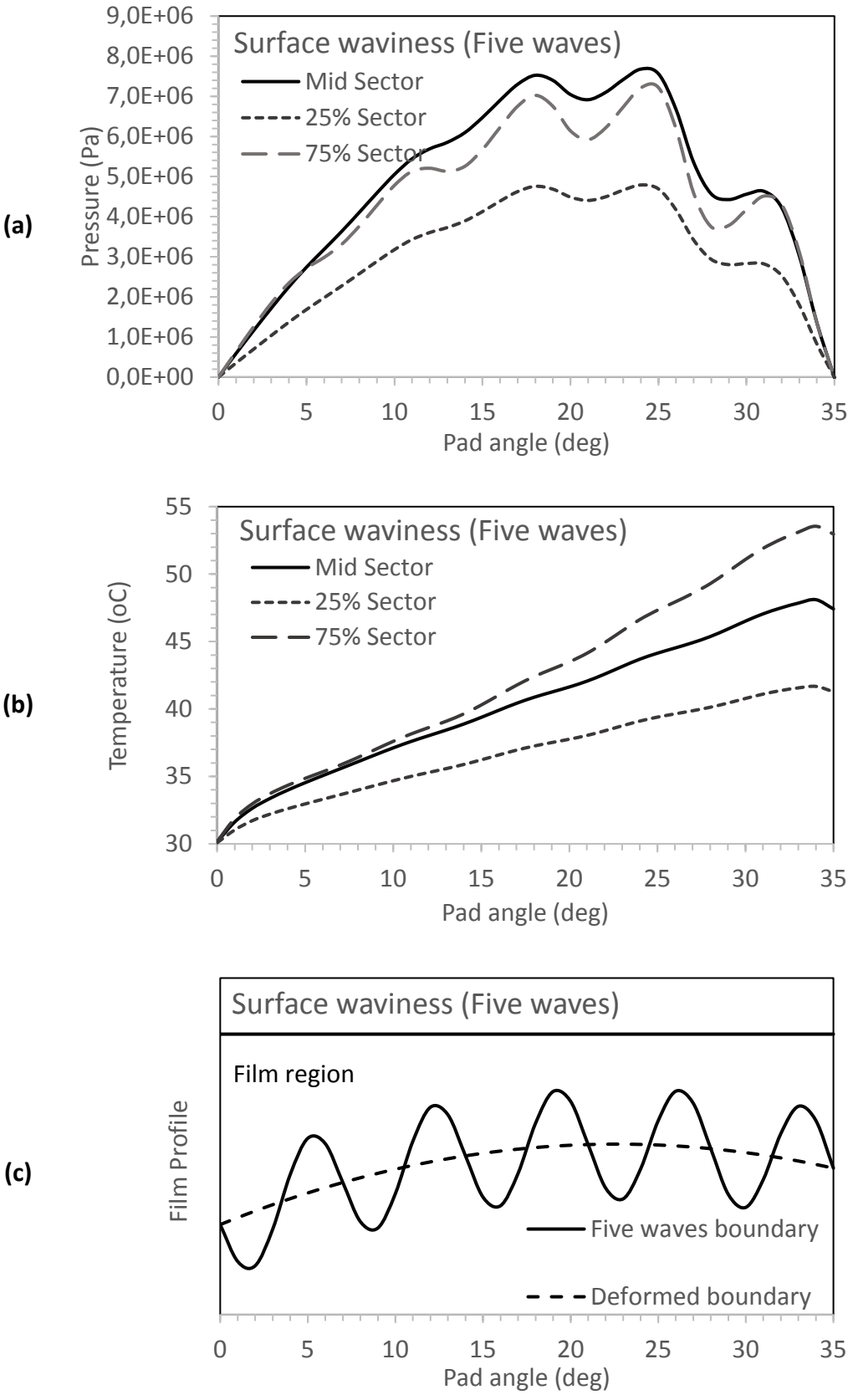

Figure 32 Three sinewave manufacturing error: (a) Pressure distributions, (b) Temperature distributions, and (c) Film profile

Finally, the contours of temperature, pressure and film thickness is being presented for the case of manufacturing errors with amplitude 20 microns.

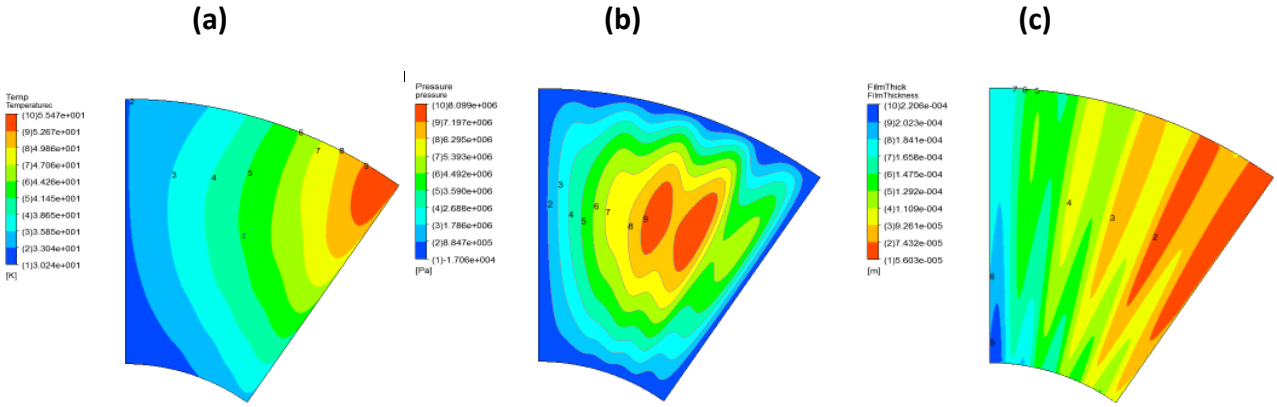

Figure 33 Contours of five sinewave: (a), (b) Temperature / pressure distribution at the babbitt-film interface, and (c) Film thickness distribution.

4.1.7 Summarized results

Comparing results in relation to the performance of the deformed pad, convexity and one sine-wave increase minimum film thickness almost 8%. On the contrary, concavity, three sine-waves and five sine-waves can decrease minimum film thickness up to 23%. In agreement with the first results convexity and one sine-wave as they increase minimum film thickness they also decrease friction torque (only 1%) and maximum temperature of the lubricant (2^{o}C). The other three cases worsen bearing performance as they increase friction torque up to 5% and maximum lubricant temperature by 10^{o}C. The above results are shown in Figure 33.

(a)

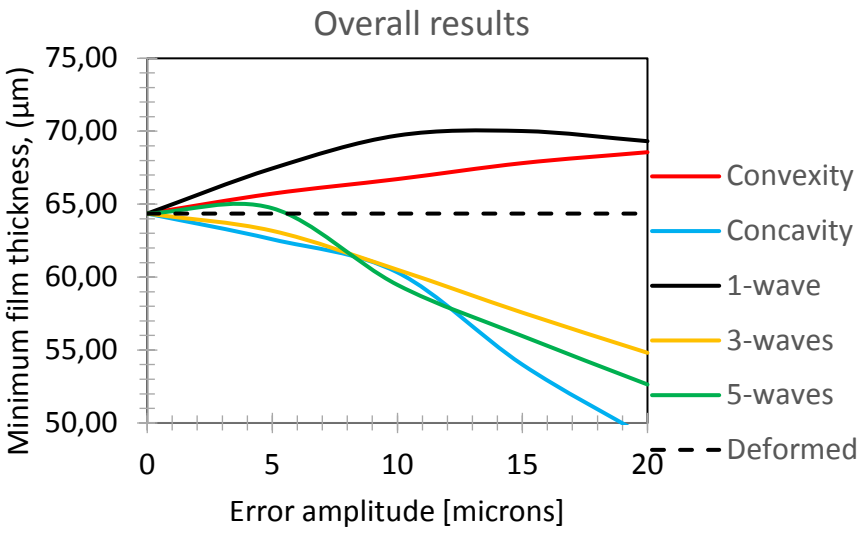

(b)

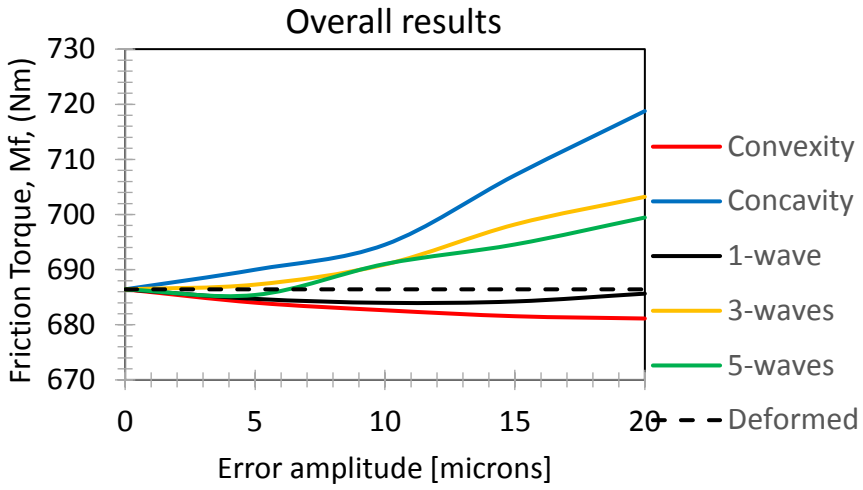

(c)

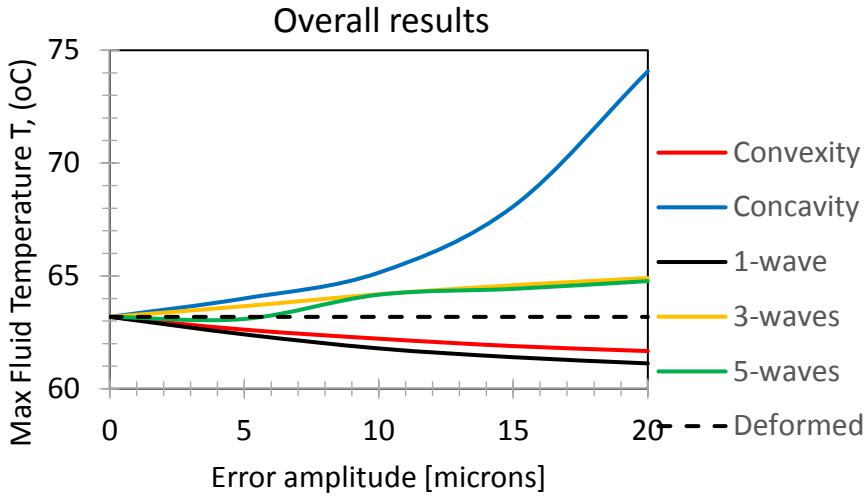

Figure 34 Summarized results of 680 kN thrust load in relation to the performance of the plain (deformed) pad bearing: (a) Minimum film thickness (b) Friction torque (c) Max fluid temperature

4.2 Thrust load of 1360 kN

4.2.1 Deformed pad geometry

In the deformed state of the pad, for load of 1360 we have assumed a constant deformation of 26 microns from plain pad across the two directions (radially, circumferentially).

In Figure 34, it is showed how the temperature of the model is being formed and also how heat power is being transferred through the solid parts.

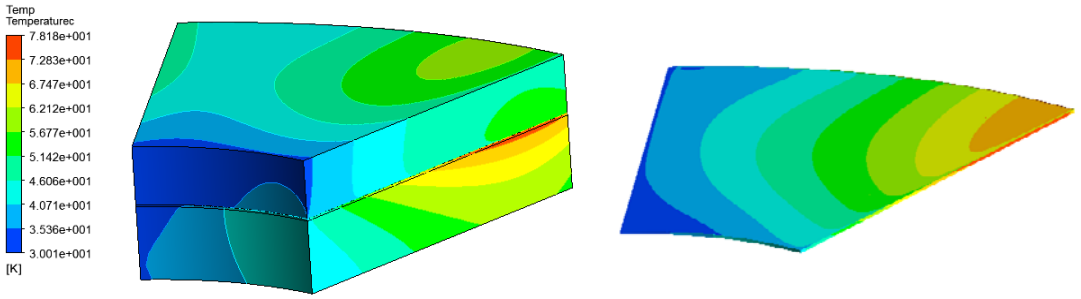

Figure 35 Temperature distribution in the lubricant and solid domains of the bearing pad.

Figure 35 (a) presents the distribution of pressure at three different positions (25% pad width, 50% pad width and 75% pad width). As shown, the highest pressure appears at the mid sector and as we get away from the mid sector the pressure decreases, mostly due to fluid leakage. Figure 35 (b) presents the distribution of temperature at the same position. In temperatures situation we see that the max temperature increases as we reach at the outer point of the pad and maximizes at the position where the H_{min} point reach (see contour of temperature). Figure 35 (c) shows the film region between pad and collar.

(a)

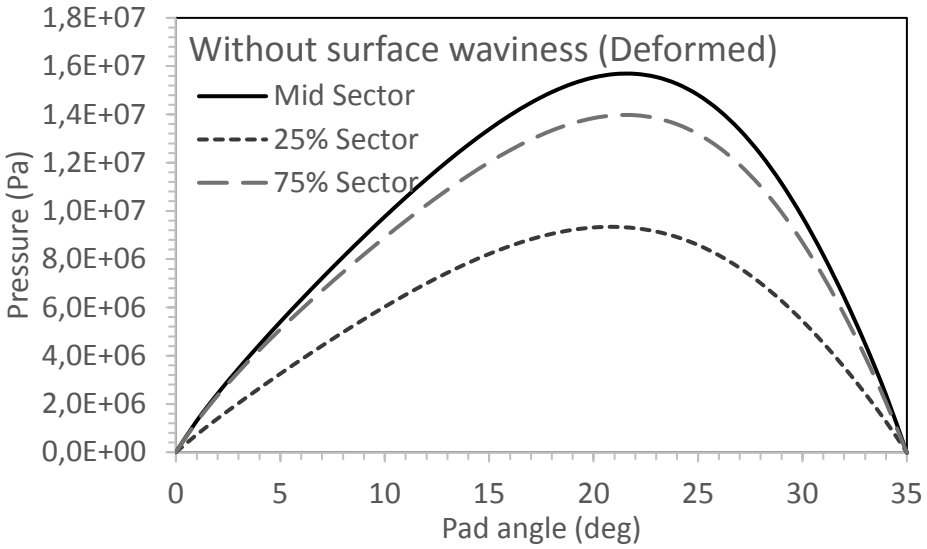

(b)

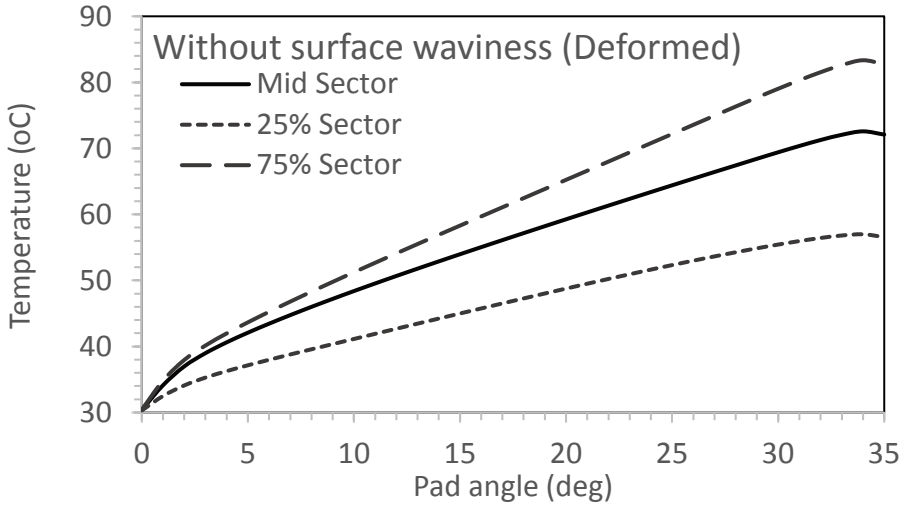

(c)

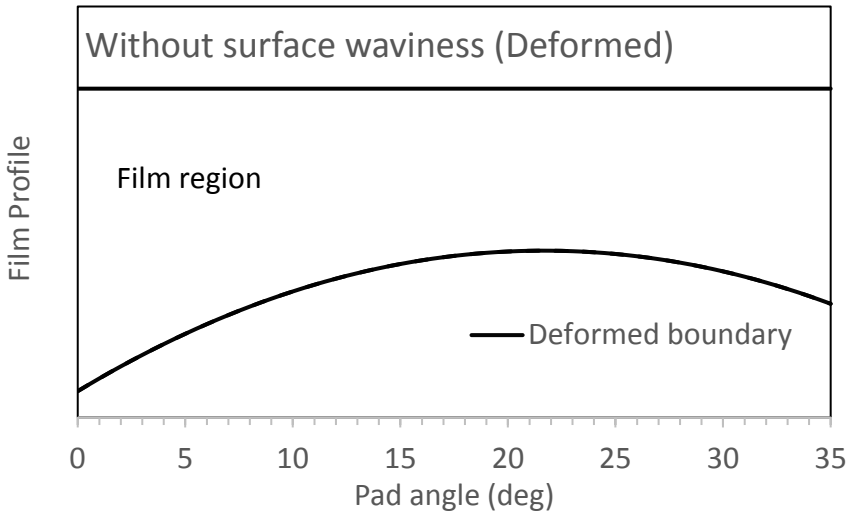

Figure 36 Deformed: (a)Chart of pressure (b)Chart of temperature (c)Film profile

In Figure 36, contour of pressure, temperature and film thickness are presented. Temperature attains a maximum at the outer region of the bearing close to the lubricant outflow. This can be attributed to the effect that collar and pad are at the closest distance and oil heating is due to viscous dissipation as well as the action of centrifugal forces. Pressure is being maximized at approximately of 65% percent of the bearing min sector (from inlet point). Minimum film thickness appears at the inflow position of pad as seen in picture below.

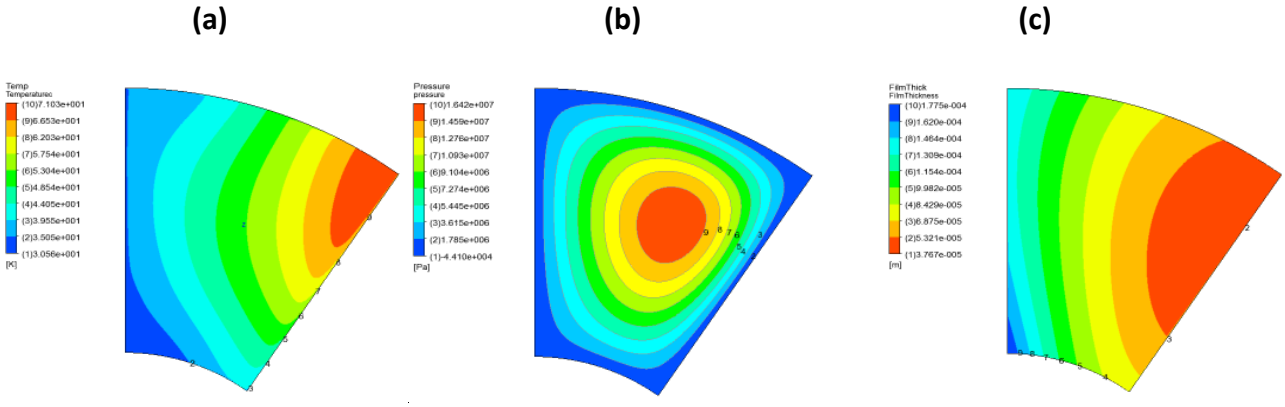

Figure 37 Contours of deformed pad: (a), (b) Temperature / pressure distribution at the babbitt-film interface, and (c) Film thickness distribution.

4.2.2 Convexity

Regarding convexity, as Figure 36 presents, minimum Film thickness increases up to 3.2%. The friction torque decreases by 1.0% and as a consequence, temperature decreases by 1.0^{o}C.

(a)

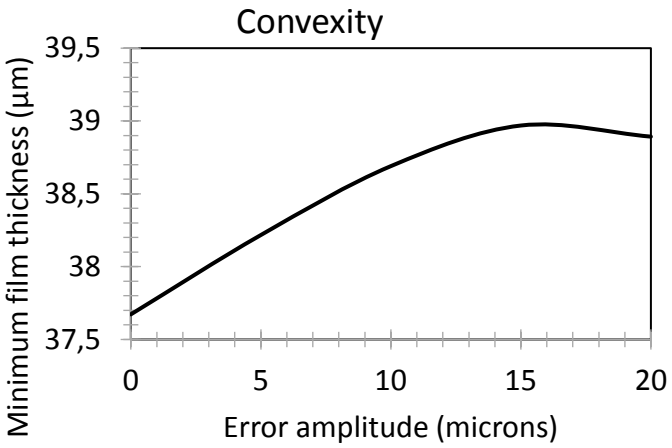

(b)

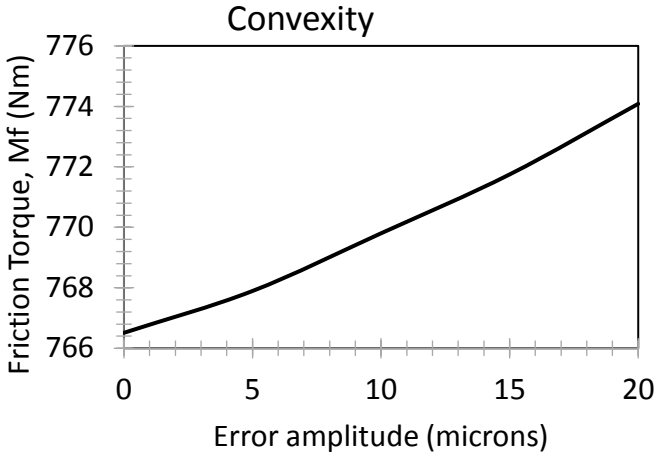

(c)

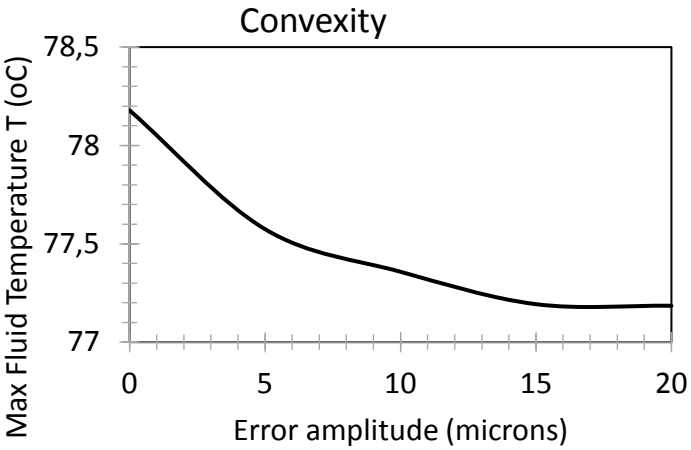

Figure 38 Performance of thrust bearing with manufacturing error "convexity" compared to the deformed bearing (a) Minimum film thickness (b) Friction torque (c) Max fluid temperature

Subsequently, the chart of pressure and temperature is being presented in Figure 38.

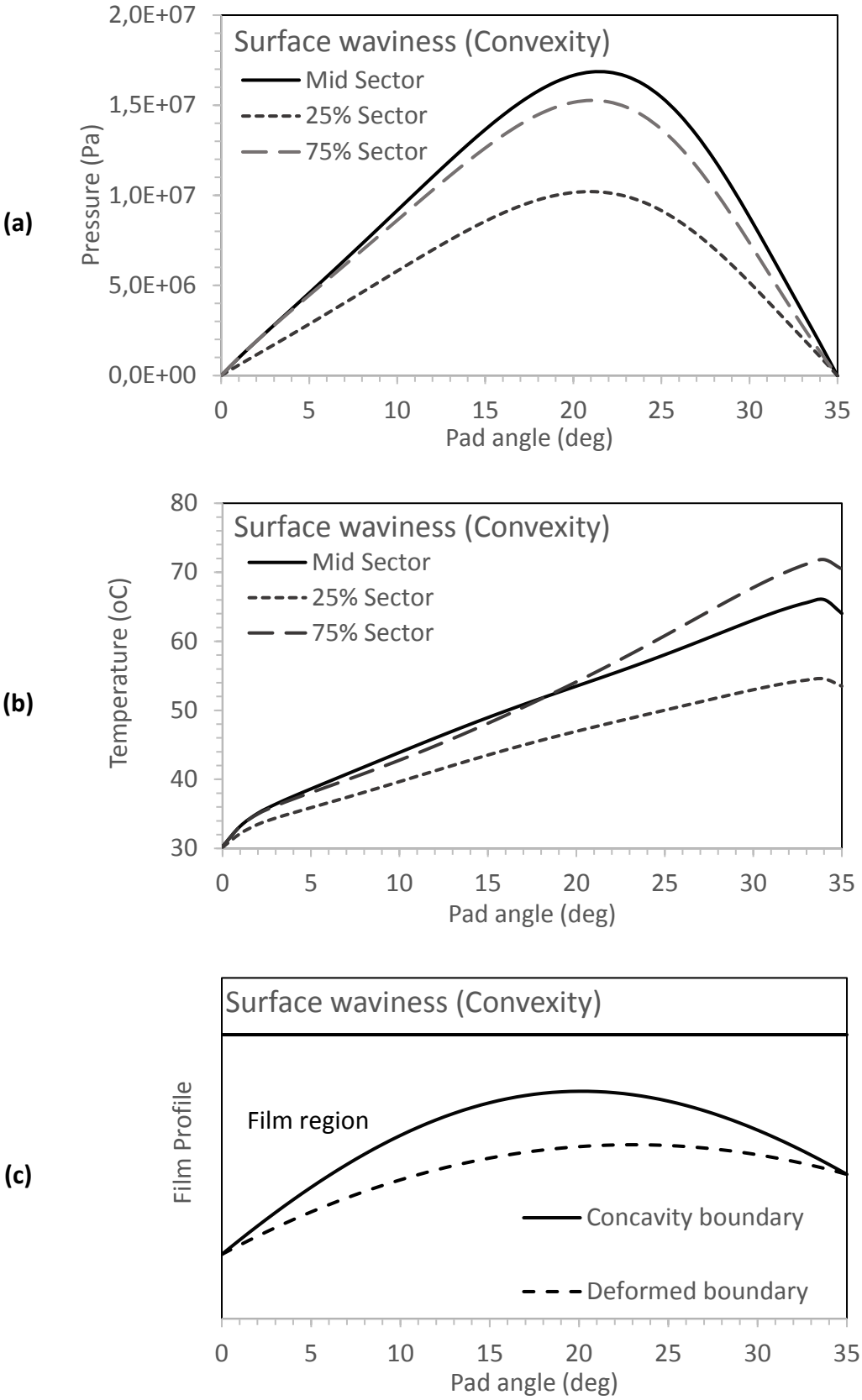

Figure 39 Convexity manufacturing error: (a) Pressure distributions, (b) Temperature distributions, and (c) Film profile

At the end, the contours of temperature, pressure and film thickness are being presented for the case of manufacturing errors with amplitude 20 microns.

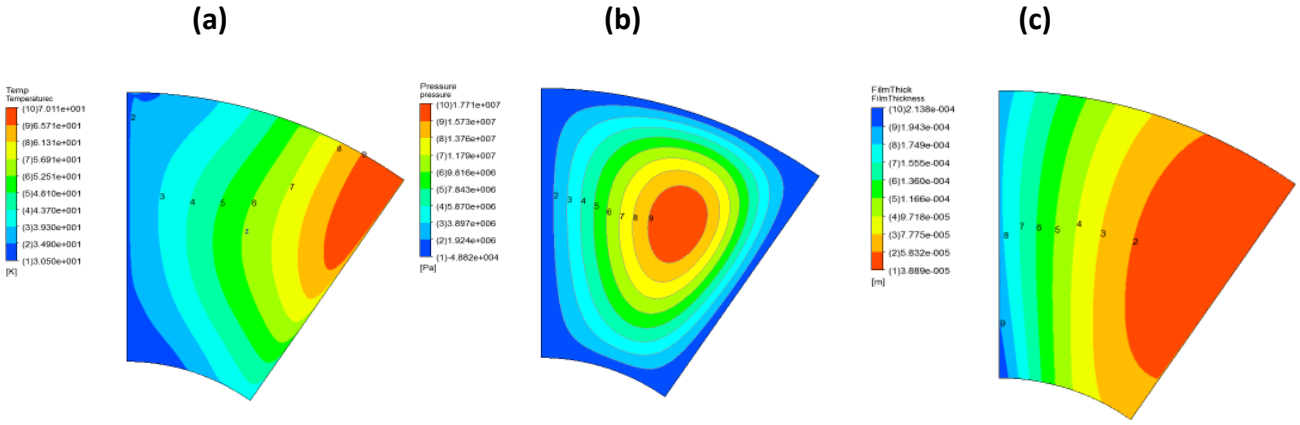

Figure 40 Contours of convexity: (a), (b) Temperature / pressure distribution at the babbitt-film interface, and (c) Film thickness distribution.

4.2.3 Concavity

Concavity affects the performance of thrust bearing as: Minimum film thickness decreases 24.9%, friction torque decreases 0.4% and temperature increases 10.0^{o}C.

(a)

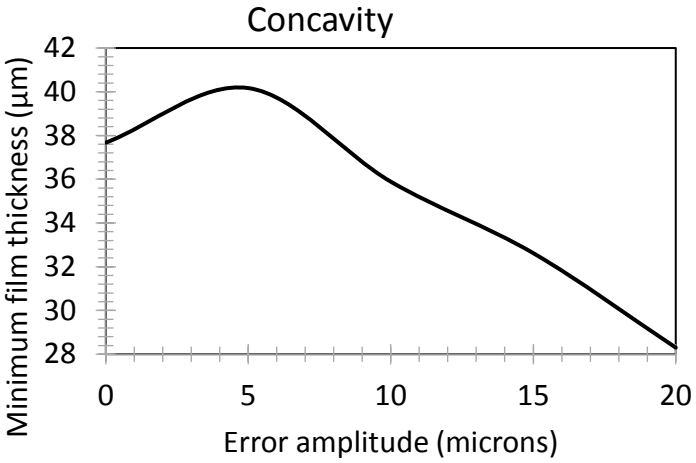

(b)

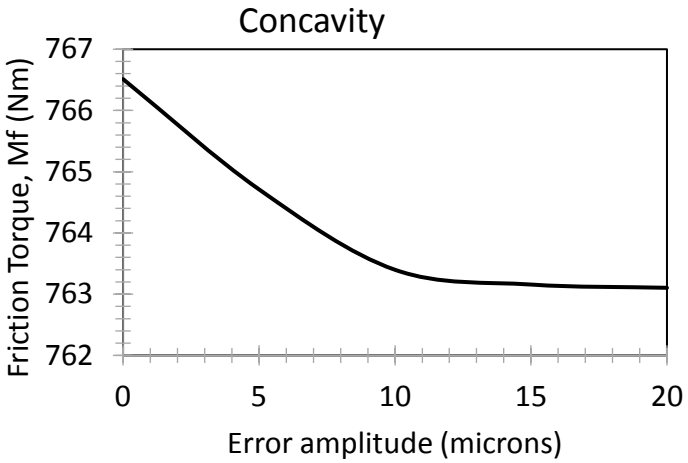

(c)

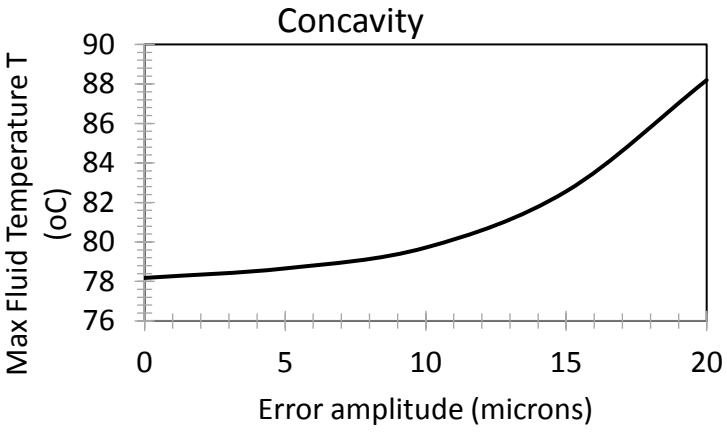

Figure 41 Performance of thrust bearing with manufacturing error "concavity" compared to the deformed bearing (a) Minimum film thickness (b) Friction torque (c) Max fluid temperature

Figure 41 presents the charts of pressure and temperature.

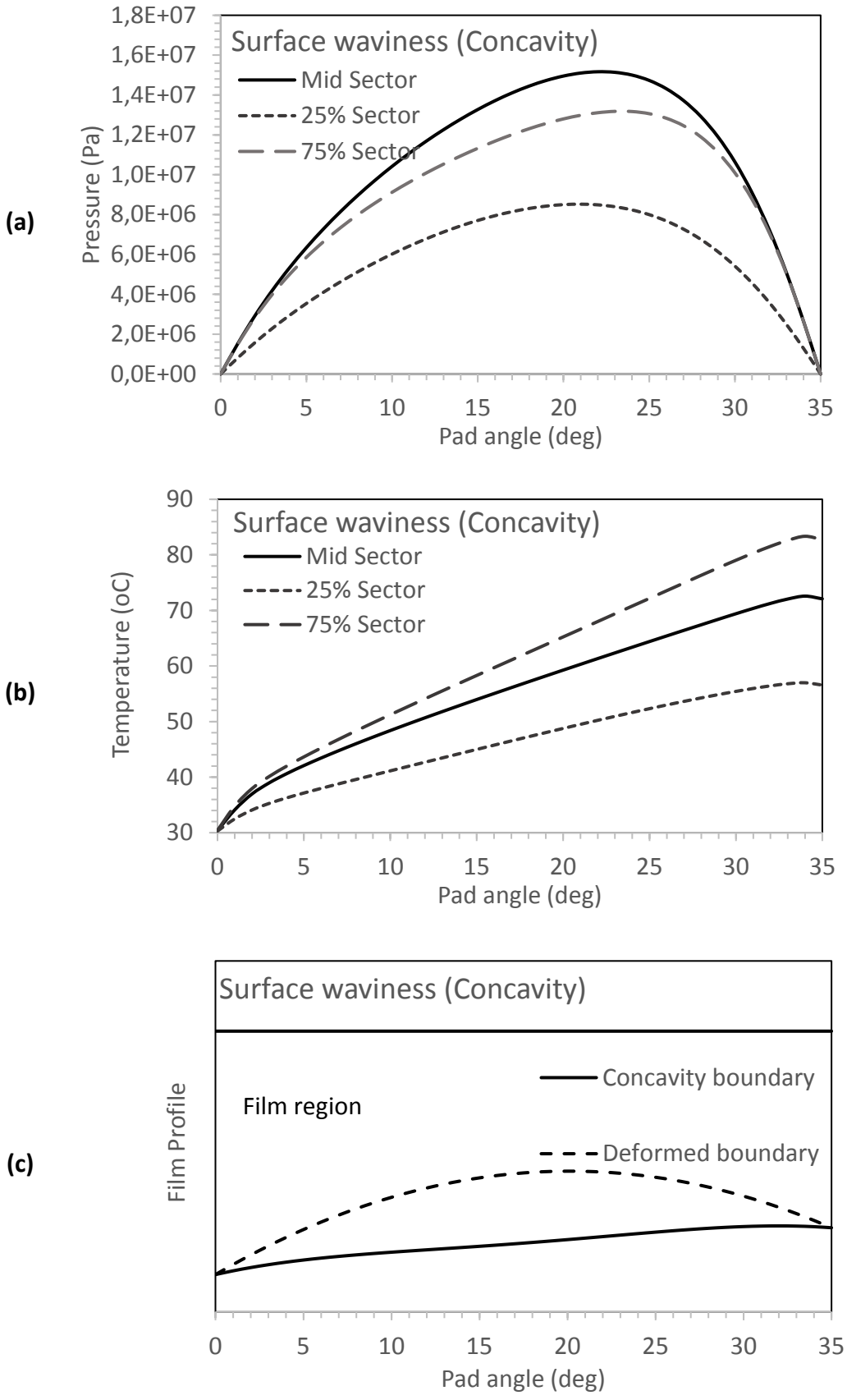

Figure 42 Concavity manufacturing error: (a) Pressure distributions, (b) Temperature distributions, and (c) Film profile

Finally, the contours of temperature, pressure and film thickness is being presented for the case of manufacturing errors with amplitude 20 microns.

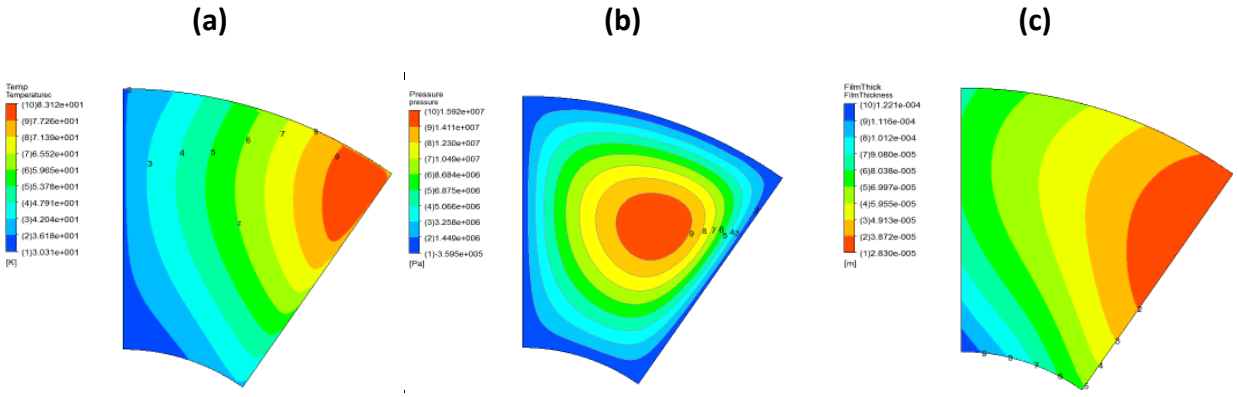

Figure 43 Contours of concavity: (a), (b) Temperature / pressure distribution at the babbitt-film interface, and (c) Film thickness distribution.

4.2.4 Waviness error - one sinewave

The influence of one sinewave in the performance of thrust bearing is: Minimum film thickness can decrease 9.2%, friction torque increase 3.2% and temperature decreases 0.3^{o}C.

(a)

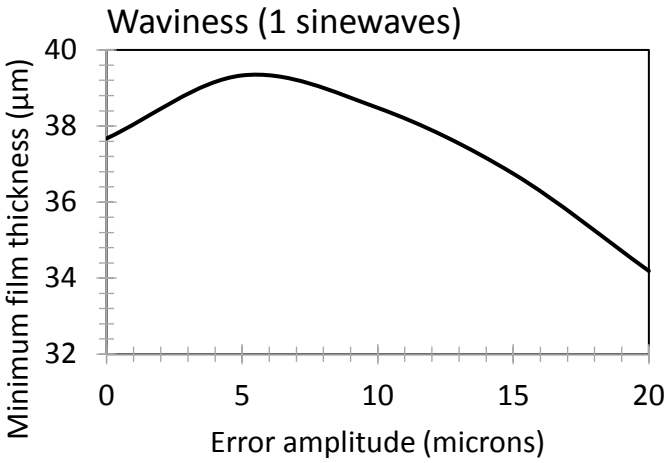

(b)

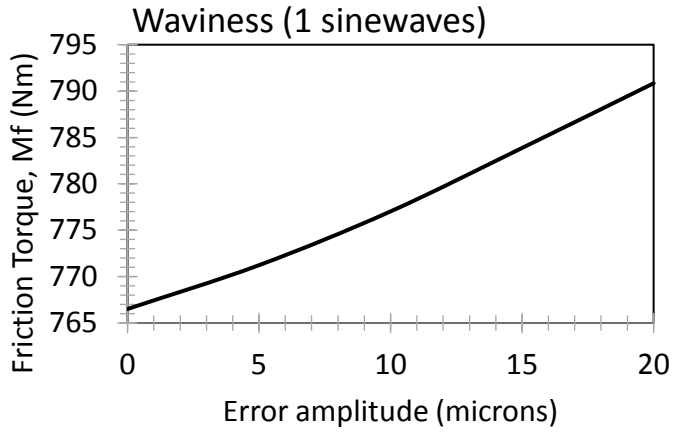

(c)

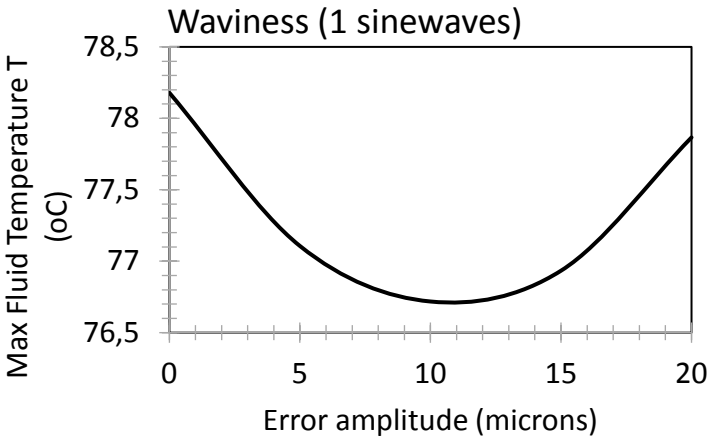

Figure 44 Performance of thrust bearing with manufacturing error "one sinewave" compared to the deformed bearing (a) Minimum film thickness (b) Friction torque (c) Max fluid temperature

In Figure bellow we see the pressure and temperature charts

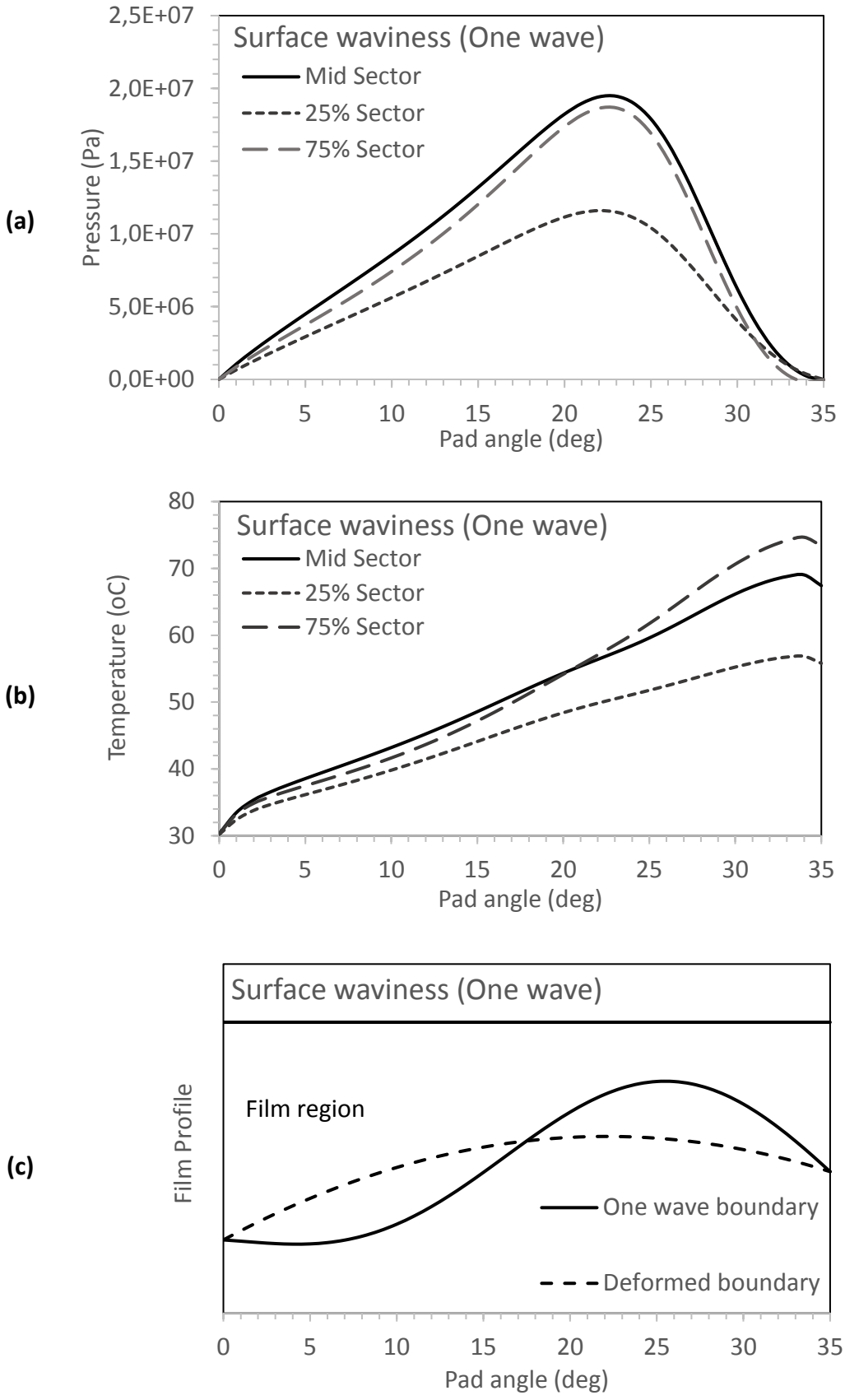

Figure 45 One sinewave manufacturing error: (a) Pressure distributions, (b) Temperature distributions, and (c) Film profile

Figure 45 presents the contours of temperature, pressure and film thickness for the case of manufacturing errors with amplitude 20 microns

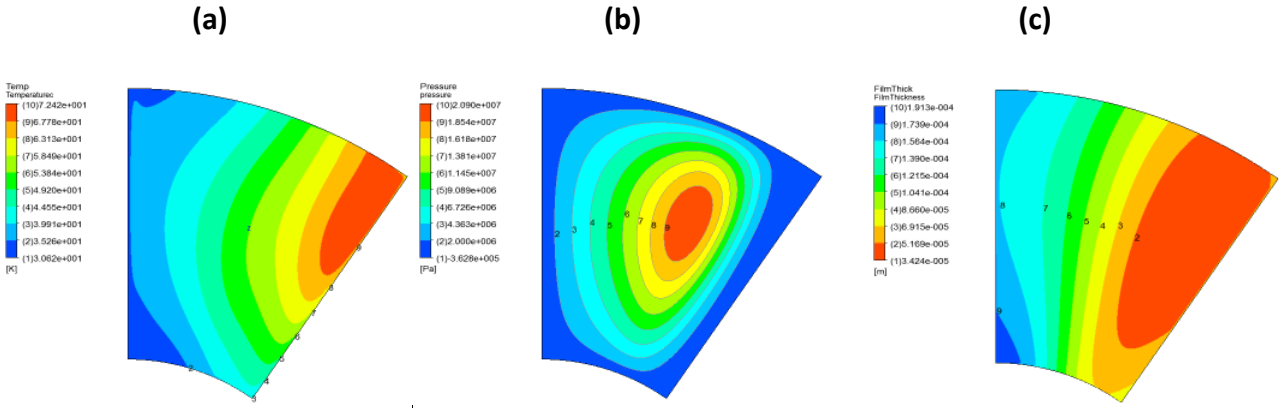

Figure 46 Contours of one sinewave: (a), (b) Temperature / pressure distribution at the babbitt-film interface, and (c) Film thickness distribution.

4.2.5 Waviness error - three sinewaves

Three sinewaves affect the performance of thrust bearing as: Minimum film thickness decreases 32.2%, friction torque increases 3.3% and temperature also increases 6.4°C.

(a)

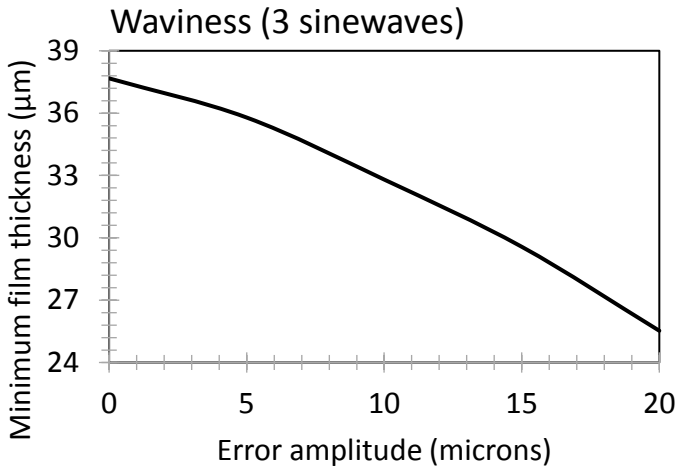

(b)

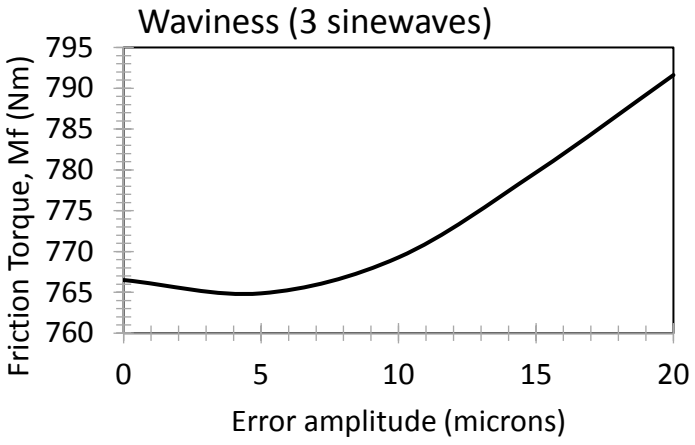

(c)

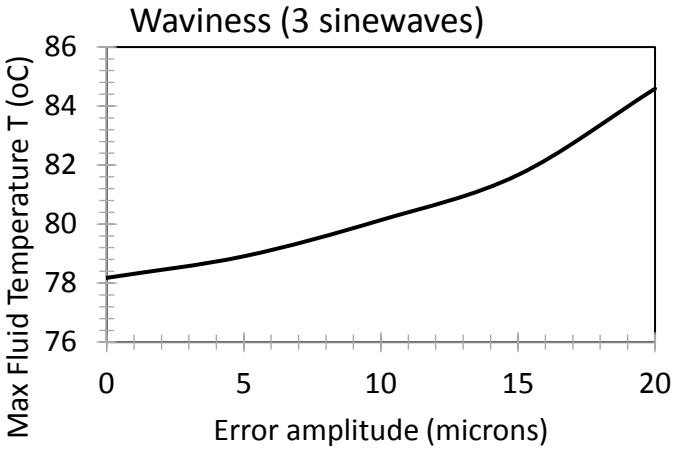

Figure 47 Performance of thrust bearing with manufacturing error "three sinewaves" compared to the deformed bearing (a) Minimum film thickness (b) Friction torque (c) Max fluid temperature

Figure 47 shows the pressure and temperature charts. From the charts we can clearly see the significant influence of the waves from the fluctuation in pressure profile. The impact in temperature profile due to waviness is negligible.

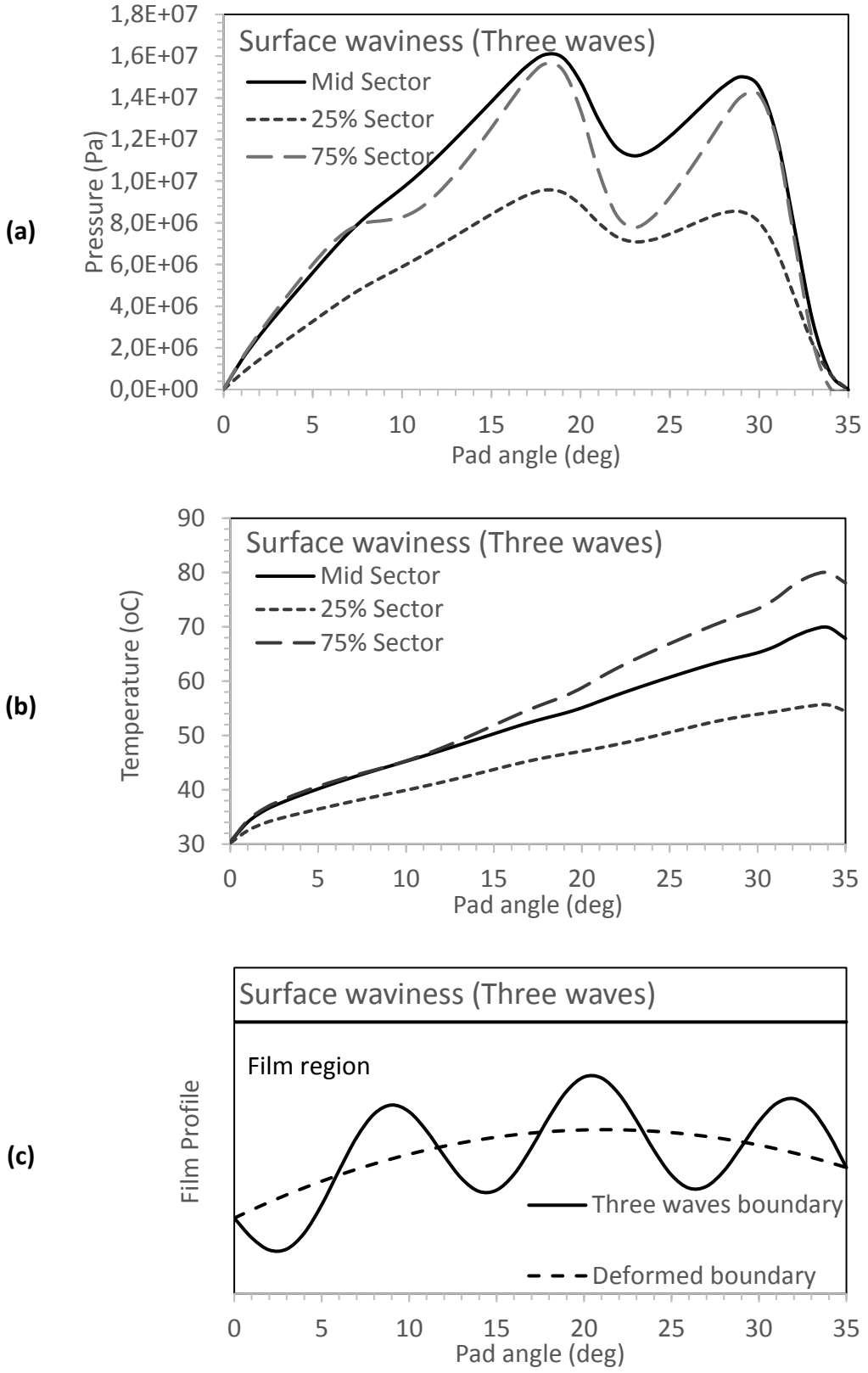

Figure 48 Three sinewave manufacturing error: (a) Pressure distributions, (b) Temperature distributions, and (c) Film profile

Finally, the contours of temperature, pressure and film thickness are being presented for the case of manufacturing errors with amplitude 20 microns.

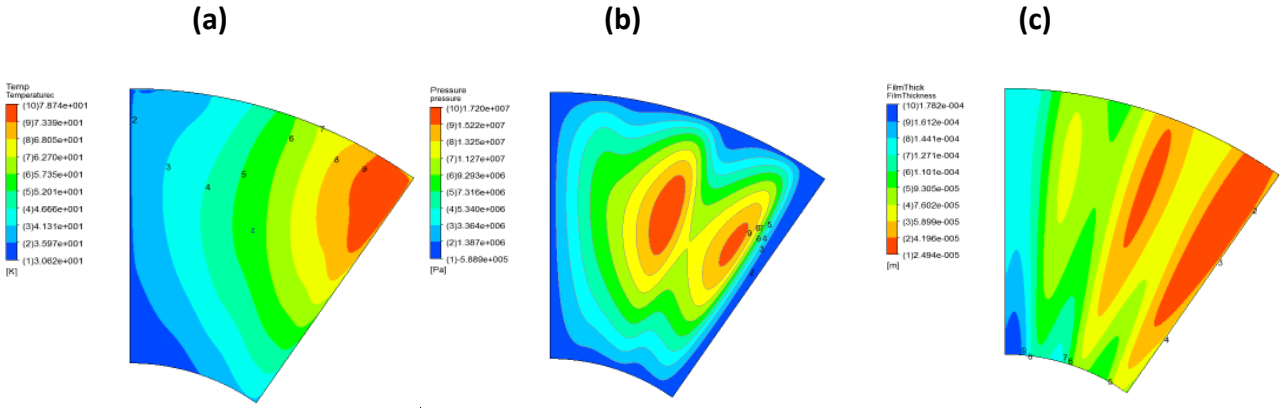

Figure 49 Contours of three sinewave: (a), (b) Temperature / pressure distribution at the babbitt-film interface, and (c) Film thickness distribution.

4.2.6 Waviness error - five sinewave

The influence of five sinewaves in the performance of thrust bearing is: Minimum film thickness decreases 37.0%, friction torque increases 3.5% and temperature also increases 5.1°C.

(a)

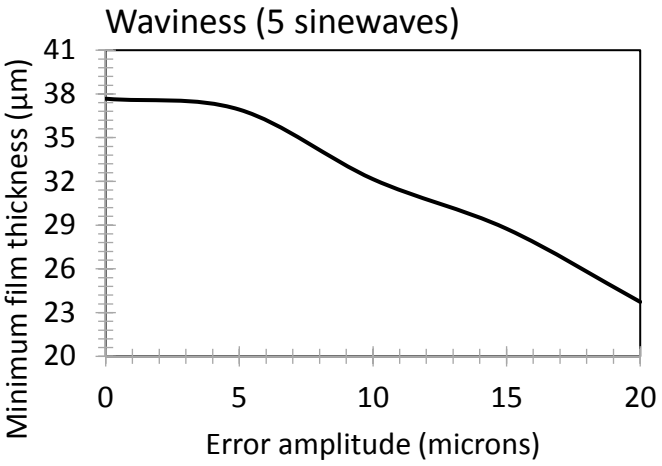

(b)

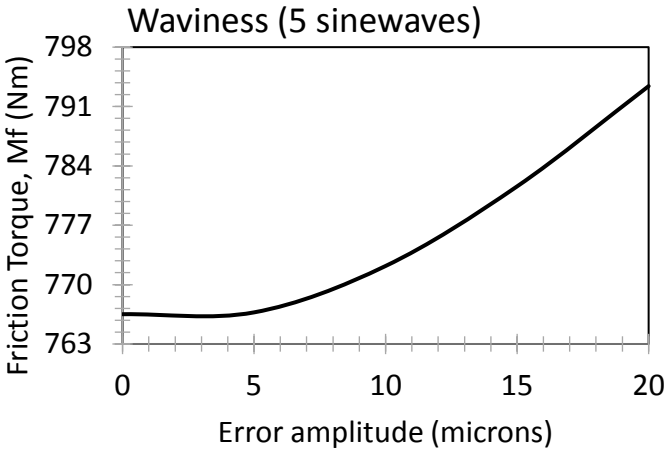

(c)

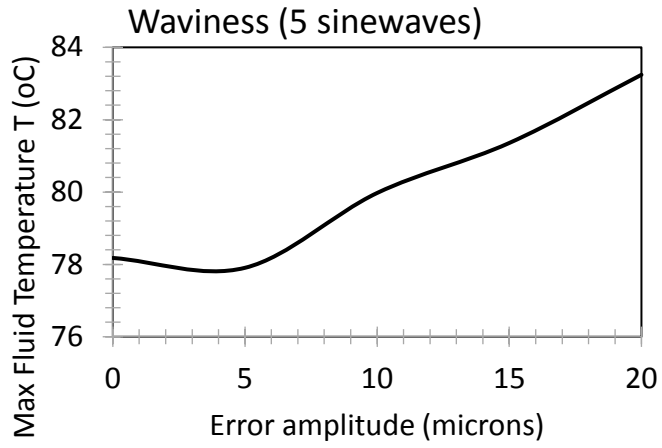

Figure 50 Performance of thrust bearing with manufacturing error "five sinewaves" compared to the deformed bearing (a) Minimum film thickness (b) Friction torque (c) Max fluid temperature

In Figure 50 we see the pressure and temperature charts. As in case of three sinewaves the influence of waviness is the same.

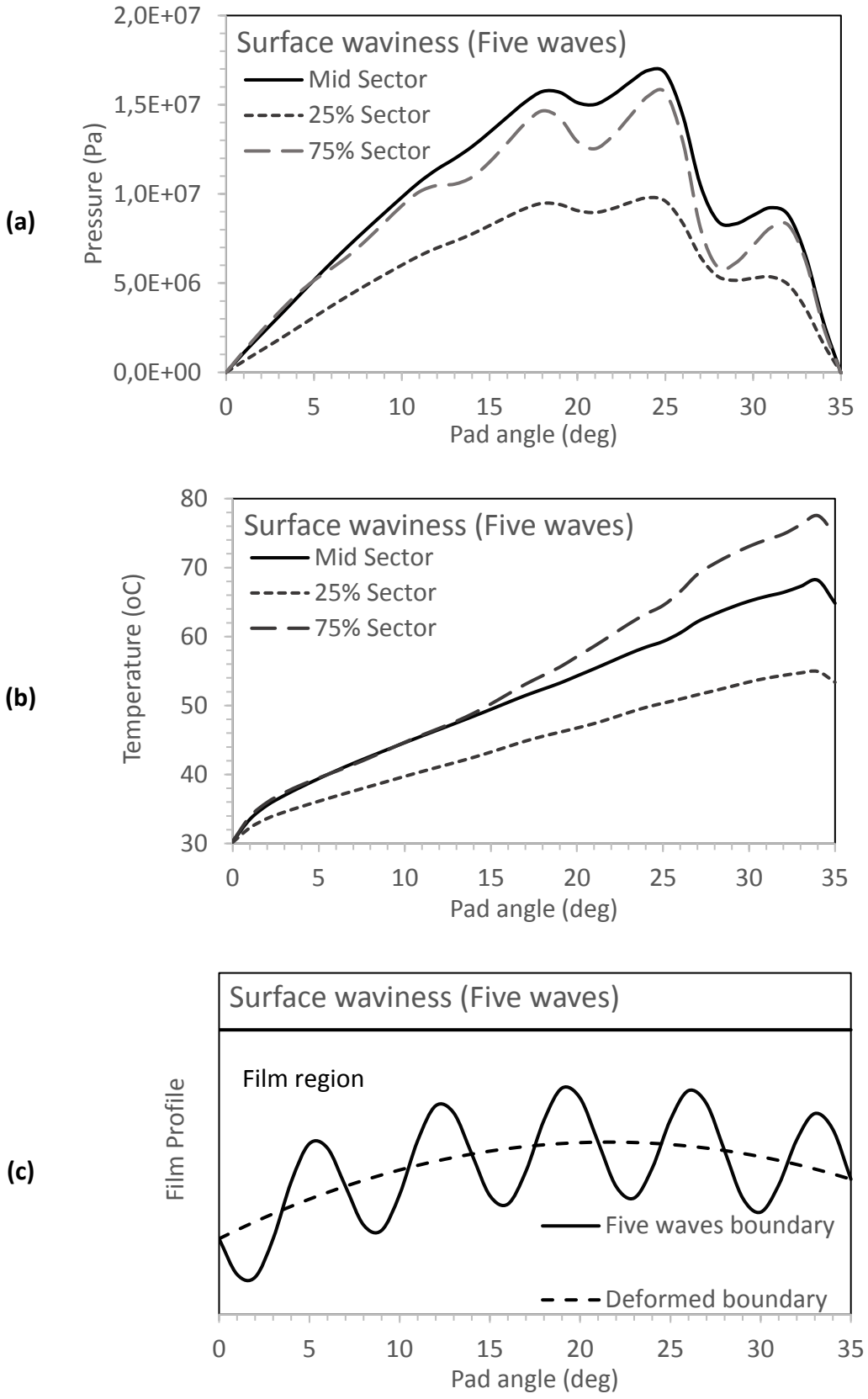

Figure 51 Three sinewave manufacturing error: (a) Pressure distributions, (b) Temperature distributions, and (c) Film profile

Finally, the contours of temperature, pressure and film thickness are being presented for the case of manufacturing errors with amplitude 20 microns.

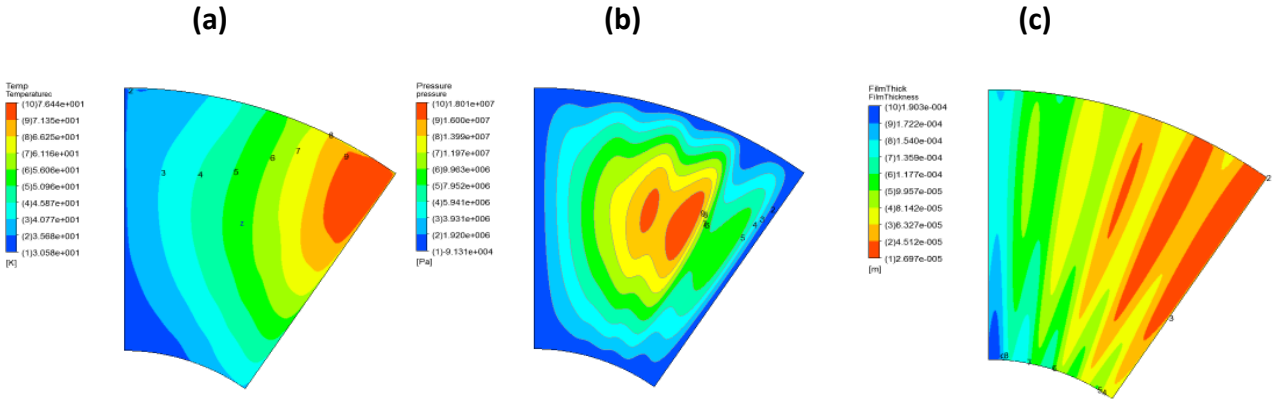

Figure 52 Contours of five sinewave: (a), (b) Temperature / pressure distribution at the babbitt-film interface, and (c) Film thickness distribution.

4.2.7 Summarized results

Comparing results in relation to the performance of the deformed pad (Figure 52), only convexity increases minimum film thickness by approximately 4%. Also, convexity decreases friction torque by 1% and maximum lubricant temperature by 1.0^{o}C. For all the other studied cases, minimum film thickness is decreased, reaching in certain cases 37%, whereas friction torque is increased by up to 4% and maximum lubricant temperature by 10.0^{o}C. However, one sine-wave seams to acts positively in max fluid temperature due to the existing space, which means that a large amount of cooled lubricant entries the film region and decreases temperature of lubricant (see Figure 44(c)), but it doesn't improve the other two crucial parameters (minimum film thickness and friction torque).

(a)

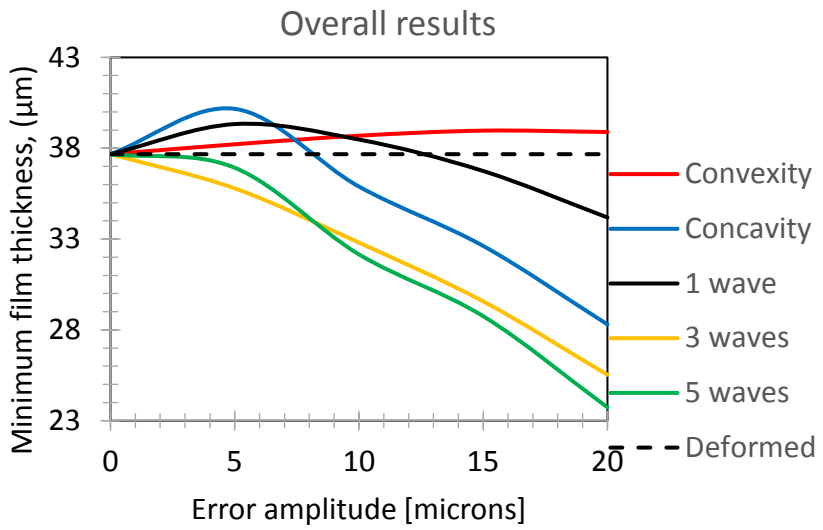

(b)

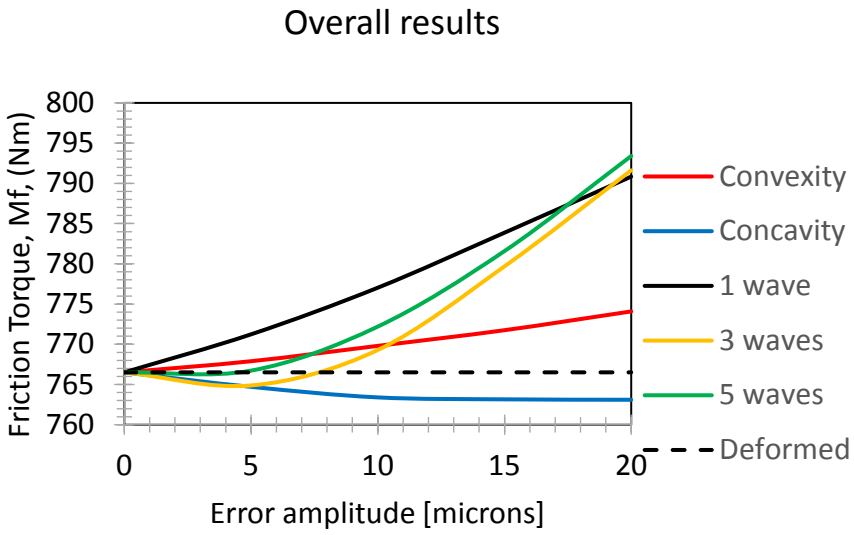

(c)

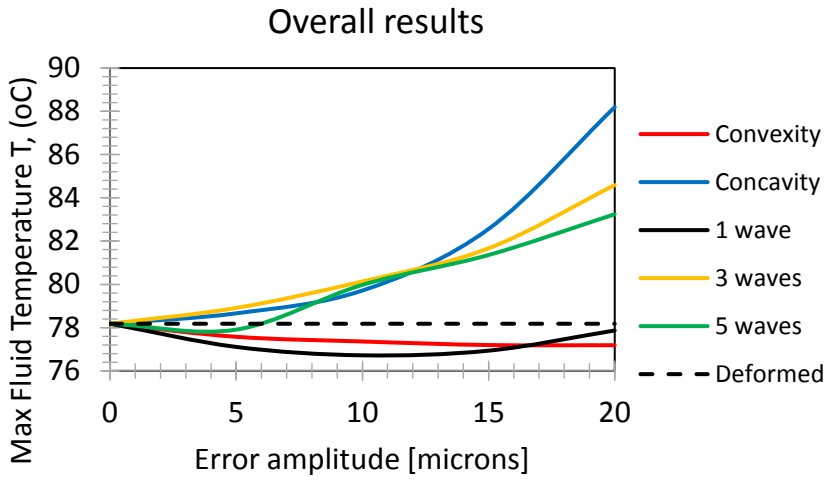

Figure 53 Summarized results of 1360 kN thrust load in relation to the performance of the plain (deformed) pad bearing: (a) Minimum film thickness (b) Friction torque (c) Max fluid temperature

5. Conclusions and Future Work

5.1 Conclusions

In the present Thesis, a computational study of tilting pad thrust bearings has been performed. The aim of the study was to investigate the influence of manufacturing errors on the performance of fluid film thrust bearings.

In particular, hydrodynamic lubrication in thrust bearing exhibiting different types of manufacturing errors at the pad surface has been considered. Three different types of manufacturing errors were studied: (a) concavity, (b) convexity, and (c) waviness (one, three or five sine-wave) of the pad surface. The main goal was to identify and quantify the (positive or negative) effect of manufacturing errors on the principal performance parameters of the bearings, in particular on minimum film thickness, load capacity, friction torque, maximum pressure and fluid temperature. Two different applied thrust loads have been considered, namely 680 kN and 1360 kN, while the rotational speed of the shaft was set at 187.5 RPM. Manufacturing errors were simulated as sinewaves, with error amplitudes ranging from 0 μm to 20 μm. Pad deformation due to elastic deformations and thermal expansion of the metallic structure we taken into consideration, based on previous literature data. The results of the present work have demonstrated that only the two of the five studied cases may lead to improved bearing operation. For the studied low thrust load (680 kN), convexity and one sinewave can increase minimum lubricant thickness and simultaneously decrease friction torque/maximum temperature of lubricant. However, for thrust load of 1360 kN, one sine-wave manufacturing error leads to worse bearing operation.

5.2 Future Work

Suggestions for future work for large tilting pad thrust bearings:

1. Implementation of manufacturing errors to the rotor surface (in addition to those of the pad surface).
2. Extension of the present THD model to account for the exact thermal expansion and elastic deformations of the bearing metallic parts, due to temperature and pressure fields.
3. Investigation of the optimal pivot position of tilting pad thrust bearings.

Literature

[1] Zouzoulas Vassilios and Papadopoulos C.I., "3-D Thermohydrodynamic Analysis Of Textured, Grooved, Pocketed And Hydrophobic Pivoted-Pad Thrust Bearings". *Tribology International* (2016): n. pag. Web.

[2] Dąbrowski, L and M Wasilczuk. "Evaluation Of Water Turbine Hydrodynamic Thrust Bearing Performance On The Basis Of Thermoelastohydrodynamic Calculations And Operational Data". *Proceedings of the Institution of Mechanical Engineers, Part J: Journal of Engineering Tribology* 218.5 (2004): 413-421. Web.

[3] Αυγερινός Ι., "Στοιχεία Μηχανών", Εκδ. Γ. Φούντας, Αθήνα, 2004.

[4] Κωστόπουλος Θ., "Οδοντώσεις και Μειωτήρες Στροφών" Εκδ. Συμεών, Αθήνα, 2010

[5] Παντελής Γ., "Μοντελοποίηση Ρυθμού Φθοράς και Βελτιστοποίηση Σχεδιασμού Ωστικών Εδράνων με Υδροφοβικές Ιδιότητες", Διπλωματική Εργασία, Ε.Μ.Π, 2013

[6] Zouzoulas V., "Thrmohydrodynamic analysis of tilting pad thrust bearings with artificial surface texturing", Athens, NTUA, 2014

[7] Raimondi, A. A., Szeri, A. Z, 1984, Journal and thrust bearings, in Handbook of Lubrication, v. II, Booser, E.R., ED., 413-462, CRC Press, Boca Raton, FL.

[8] Gardner, W. W., 1988, "Tilting-pad thrust bearing tests, influence of pivot location", ASME Journal of Tribology., 110(4), pp.609-613

[9] Shinkle, J. N., Hornung, K. G., 1965, "Frictional Characteristics of Liquid Hydrostatic Journal Bearings", ASME Journal of Basic Engineering, Vol. 87, Issue1, pp. 163-169

[10] Fillion, M., Glavatskih, S.B., 2008. "PTFE-faced Centre Pivot Thrust Pad Bearings: Factors Affecting TEHD Performance." Tribology International 41(12), pp. 1219-1225

[11] Παυλιογλου Σ., "Βελτιστοποίηση τριβολογικής συμπεριφοράς ωστικών εδράνων λιπαινόμενων με ηλεκτρορεολογικά ρευστά", Διπλωματική Εργασία, Ε.Μ.Π, 2013

[12] Charitopoulos, A., Efstathiou, E., Papadopoulos, C., Nikolakopoulos, P. and Kaiktsis, L. (2013). Effects of manufacturing errors on tribological characteristics of 3-D textured micro- thrust bearings. *CIRP Journal of Manufacturing Science and Technology*, 6(2), pp.128-142.

[13] Wasilczuk, M. & Rotta, G. 2013. On the Possibilities of Decreasing Power Loss in Large Tilting Pad Thrust Bearings. *ISRN Tribology*, 2013: 1-9.

[14] Wasilczuk, M. & Rotta, G. 2008. Modeling lubricant flow between thrust-bearing pads. *Tribology International*, 41(9-10): 908-913.

[15] Wasilczuk, M., Wodtke, M., & Braun, W. 2015. Centrally Pivoted Tilting Pad Thrust Bearing with Carbon-Based Coated Collar—Experimental Results of Low- and Medium-Speed Operation. *Tribology Transactions*, 58(5): 882-893.

[16] Wodtke, M., Olszewski, A., & Wasilczuk, M. 2013. Application of the fluid-structure interaction technique for the analysis of hydrodynamic lubrication

problems. *Proceedings of the Institution of Mechanical Engineers, Part J: Journal of Engineering Tribology*, 227(8): 888-897.

[17] Pajaczkowski, P., Schubert, A., Wasilczuk, M., & Wodtke, M. 2013. Simulation of large thrust-bearing performance at transient states, warm and cold start-up. *Proceedings of the Institution of Mechanical Engineers, Part J: Journal of Engineering Tribology*, 228(1): 96-103.

[18] Burton R.A.: Effect of two dimensional sinusoidal roughness on the load support characteristics of a lubricant film. *Journal of Basing Engineering*, Vol. 85 (2), 1963, pp. 258 – 265.

[19] Li J., Chen H.S.: Evaluation on applicability of Reynolds equation for squared transverse roughness compared to CFD. *Journal of Tribology* - Transactions of ASME, Vol. 129 (4), 2007, pp. 963 – 967.

[20] Pande S.S., Somasundaram S.: Effect of manufacturing errors on the performance of aerostatic journal bearings Wear, Vol. 66 (2), 1981, pp. 145 – 156.

[21] Wilson D.: The Effect of Geometry Variations on Hydrodynamic Bearing Performance. ASLE Transactions, Vol. 9 (4), 1966, pp. 411-419.

[22] Shelly P., Ettles C.: Effect of Transverse and Longitudinal Surface Waviness on the Operation of Journal Bearings. *Journal of Mechanical Engineering Science*, Vol. 14, Issue 3, 1972, pp. 168 – 172.

[23] Berthe D., Fantino B., Frene J., Godet M.: Influence of Shape Defects and Surface Roughness on the Hydrodynamics of Lubricated Systems. *Journal Mechanical Engineering Science*, IMechE, Vol. 16 (3), 1974, pp. 156-159.

[24] Frene J., Nicolas D., Degueurce B., Berthe D., Godet M.: Hydrodynamic Lubrication, Volume 33, Bearings and Thrust Bearings. Elsevier Science, 1997.

[25] Fillon M., Bouyer J.: *Thermohydrodynamic analysis of a worn plain journal bearing*. Tribology International, Vol. 37, 2004, pp. 129-136.

[26] Litwin W.: Influence of local bush wear on water lubricated sliding bearing load carrying capacity. Tribology International, Vol. 103, 2016, pp. 352-358.

[27] Dobrica M.B., Fillon M.: Performance degradation in scratched journal bearing. *Tribology International*, Vol. 51, 2012, pp. 1-10.

[28] Papadopoulos, C. I.; Kaiktsis, L.; Fillon, M.: Computational fluid dynamics thermohydrodynamic analysis of three-dimensional sector-pad thrust bearings with rectangular dimples. *Journal of Tribology* - Transactions of ASME, Vol. 136 (1), 2014, 011702.

[29] Fouflias D.G., Charitopoulos A.G, Papadopoulod C.I., Kaiktsis L., Fillon M.: Performance Comparison Between Textured, Pocket, and Tapered-land Sector-Pad Thrust Bearings Using Computational Fluid Dynamics Thermohydrodynamic Analysis. *Proceedings of the Institution of Mechanical Engineers Part J-Journal of Engineering Tribology*, Vol. 229 (4), 2015, pp 376 – 397.

[30] Fillon M., Wodtke M., Wasilczuk M.: Effect of Presence of Lifting Pocket on the THD Performance of a Large Tilting-pad Thrust Bearing. Friction, Vol. 3 (4), 2015, pp. 266 – 274.

[31] De Pellegrin D.V., Hargreaves D.J.: An isoviscous, isothermal model investigating the influence of hydrostatic recess on a spring-supported tilting pad thrust bearing. *Tribology International*, Vol. 51, 2012, pp. 25-35.

[32] Roylance B.J.: Radially Grooved Thin Plate Thrust Washers: Factor Affecting Their Performance*. Journal of Lubrication Technology* - Transactions of ASME, Vol. 97 (4), 1975, pp. 565 – 569.